National Library of Canada
Acquisitions and Bibliographic Services Branch
395 Wellington Street
Ottawa, Ontario
K1A 0N4

Bibliothèque nationale du Canada
Direction des acquisitions et des services bibliographiques
395, rue Wellington
Ottawa (Ontario)
K1A 0N4

Your file *Votre référence*

Our file *Notre référence*

NOTICE

The quality of this microform is heavily dependent upon the quality of the original thesis submitted for microfilming. Every effort has been made to ensure the highest quality of reproduction possible.

If pages are missing, contact the university which granted the degree.

Some pages may have indistinct print especially if the original pages were typed with a poor typewriter ribbon or if the university sent us an inferior photocopy.

Reproduction in full or in part of this microform is governed by the Canadian Copyright Act, R.S.C. 1970, c. C-30, and subsequent amendments.

AVIS

La qualité de cette microforme dépend grandement de la qualité de la thèse soumise au microfilmage. Nous avons tout fait pour assurer une qualité supérieure de reproduction.

S'il manque des pages, veuillez communiquer avec l'université qui a conféré le grade.

La qualité d'impression de certaines pages peut laisser à désirer, surtout si les pages originales ont été dactylographiées à l'aide d'un ruban usé ou si l'université nous a fait parvenir une photocopie de qualité inférieure.

La reproduction, même partielle, de cette microforme est soumise à la Loi canadienne sur le droit d'auteur, SRC 1970, c. C-30, et ses amendements subséquents.

Canada

UNIVERSITY OF ALBERTA

AN IMPEDANCE MODEL FOR THE ASSESSMENT OF GASTRIC EMPTYING

BY

ROLAND MAH ©

A THESIS SUBMITTED TO THE FACULTY OF GRADUATE STUDIES AND RESEARCH IN PARTIAL FULFILMENT OF THE REQUIREMENTS FOR THE DEGREE OF MASTER'S OF SCIENCE

DEPARTMENT OF ELECTRICAL ENGINEERING

EDMONTON, ALBERTA

FALL 1992

National Library of Canada
Bibliothèque nationale du Canada

Canadian Theses Service
Service des thèses canadiennes

Ottawa, Canada
K1A 0N4

The author has granted an irrevocable non-exclusive licence allowing the National Library of Canada to reproduce, loan, distribute or sell copies of his/her thesis by any means and in any form or format, making this thesis available to interested persons.

The author retains ownership of the copyright in his/her thesis. Neither the thesis nor substantial extracts from it may be printed or otherwise reproduced without his/her permission.

L'auteur a accordé une licence irrévocable et non exclusive permettant à la Bibliothèque nationale du Canada de reproduire, prêter, distribuer ou vendre des copies de sa thèse de quelque manière et sous quelque forme que ce soit pour mettre des exemplaires de cette thèse à la disposition des personnes intéressées.

L'auteur conserve la propriété du droit d'auteur qui protège sa thèse. Ni la thèse ni des extraits substantiels de celle-ci ne doivent être imprimés ou autrement reproduits sans son autorisation.

ISBN 0-315-77277-8

Canada

UNIVERSITY OF ALBERTA

RELEASE FORM

NAME OF AUTHOR: Roland Mah

TITLE OF THESIS: An Impedance Model for the Assessment of Gastric Emptying

DEGREE: Master's of Science

YEAR THIS DEGREE GRANTED: 1992

Permission is hereby granted to the University of Alberta Library to reproduce single copies of this thesis and to lend or sell such copies for private, scholarly or scientific research purposes only.

The author reserves all other publication and other rights in association with the copyright in the thesis, and except as hereinbefore provided neither the thesis nor any substantial portion thereof may be printed or otherwise reproduced in any material form whatever without the author's prior written permission.

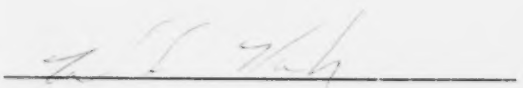

10570-31 Ave

Edmonton, Alberta

T6J 2Y3

26 May 1992

UNIVERSITY OF ALBERTA

FACULTY OF GRADUATE STUDIES AND RESEARCH

The undersigned certify that they have read, and recommend to the Faculty of Graduate Studies and Research for acceptance, a thesis entitled AN IMPEDANCE MODEL FOR THE ASSESSMENT OF GASTRIC EMPTYING submitted by Roland Mah in partial fulfillment of the requirements for the degree of Master's of Science in Biomedical Engineering.

Dr. Y. J. Kingma
Supervisor

Dr. K. L. Bowes
Committee Member

Dr. V. G. Gourishankar
Committee Member

Date: July 2 - 1992

ABSTRACT

Noninvasive impedance methods producing an image were initially examined. The images were of a cross-sectional plane in the human body. Since the resolution of the images was poor, impedance methods were then examined as a way to assess gastric emptying.

Four models were developed which allow precise determination of impedances.

The square resistor-array model provides maximum flexibility in shape of the human torso. Since it is an analog model, impedances can be measured directly.

To better approximate the human torso, this model was modified into a circular-array. Impedances measured on this model were more conclusive, since the circular array eliminated the effects of resistors on the corners of the square array.

The third model was a computer simulation based on the previous model. Impedances could now be calculated in a fraction of the time it took to measure them on the analog models. It was also easier to change configurations in the computer model than in the analog models.

Finally, an electrolytic model was developed. This would better approximate the more continuous set of impedances found in the human torso, as opposed to the discrete impedances of the previous models. Results from this necessitated some changes in the previous models;

specifically the use of one-deep probes and normalization by length of the diagonal.

Once these changes were implemented, computer simulation showed how the impedance method can be used to assess gastric emptying.

IMPEDANCE MODEL FOR THE ASSESSMENT OF GASTRIC EMPTYING

Table of Contents

I. Introduction 1

II. Background 2
A. Impedance Computed Tomography (ICT) 3
B. Biological Properties of Tissue 4
C. Terms and Definitions 6
D. Statement of Problem 8
E. Approaches to Impedance Imaging 13
F. Problems with ICT Imaging 21
G. Physical Factors in Constructing ICT Systems 26
H. ICT Prototype Systems 29
I. Applications of ICT 33
J. Summary 36

III. Experimentation 38
A. The Square Resistor Array Model 38
B. The Circular Resistor Array Model 55
C. The Computer Model 67
D. The Electrolytic Model 99
E. Modifications to the Resistor Board Model ...105

IV. Assessment of Gastric Emptying 123

V. Conclusion 127

Footnotes 129

Bibliography 131

Appendix 133

List of Tables

Table 1: A survey of published resistivity values for mammalian tissue 5

Table 2: The computed values of impedances and the differences in impedance between computed and measured values 79

List of Figures

Figure 1: Basic configuration used in Impedance Computed Tomography 3

Figure 2: Small conductive region embedded within large conductive region 6

Figure 3: The computer model (Yorkey and Webster) 17

Figure 4: The error in each iteration for the six methods (Yorkey and Webster) 18

Figure 5: The time for one iteration of each method (Yorkey and Webster) 19

Figure 6: The error in the reconstructed image after one iteration (Yorkey and Webster) 20

Figure 7: Electrode carrier for CT-Imaging showing the Effective Measurement Zones 23

Figure 8: Image from simple back-projection of the change in resistivity between inhalation and exhalation 24

Figure 9: Graph of peak image amplitude against distance of point from array 25

Figure 10: The functional block diagram of the overall impedance imaging system 29

Figure 11: Block diagram showing electrodes around a body and multiplexing electronics 32

Figure 12: A resistivity cross section of an arm 32

Figure 13: An applied potential tomographic image of a forearm constructed from a 16-electrode circular array 33

Figure 14: Diagrammatic cross section of the forearm 34

Figure 15: Single cell of the square resistor array model 39

Figure 16: A sample a) row, b) column, c) left-top diagonal, and d) right-top diagonal in the square resistor array model ..44

Figure 17: Locations of the single-cell anomaly in the square resistor array model 48

Figure 18: Impedances of a) rows, b) columns, c) left-top diagonals and d) right-top diagonals in the square resistor array 49

Figure 19: Differences in impedances measured between single-cell anomalies and no anomaly 50

Figure 20: Difference in impedances measured divided by the number of cells in the diagonal 51

Figure 21: Normalized impedances of a) rows, b) columns, c) left-top diagonals, and d) right-top diagonals 52

Figure 22: Total differences in impedances for the configuration with the R5C17 anomaly 53

Figure 23: Configuration of the circular resistor array model with diagonals 1 and 2 indicated 56

Figure 24: Current path lines diverging around an object of high impedance (continuous medium) 57

Figure 25: Impedance measurements for the circular resistor array model 61

Figure 26: The diagonals which had the highest impedances measured for each anomaly 62

Figure 27: Currents and resistances of a single cell in the square resistor array model 68

Figure 28: Diagonal impedances of the circular resistor array model when the single anomaly has five times the resistance of the other cells 82

Figure 29: the impedances calculated as the single-cell anomaly is moved along row 10 86

Figure 30: the six layers in the model. An anomaly passing between layers causes an increase in impedance of approximately 0.1 k ohms. 87

Figure 31: location of the single multiple-celled anomaly 91

Figure 32: computed impedances as the anomaly contracts one column at a time 92

Figure 33: the three different sizes in the anomaly 96

Figure 34: computed impedances as the anomaly's radius changes 97

Figure 35: measured impedances for the electrolyte (continuous) model containing a circular, continuous anomaly with a diameter of one-quarter the diameter of the model 103

Figure 36: one-deep probe locations in the circular model 112

Figure 37: computed impedances for the 13-cell anomaly when probes are located one layer from the edge of the array, both before and after normalization 113

Figure 38: computed impedances for the one-cell anomaly when probes are located one layer from the edge of the array, both before and after normalization 114

Figure 39: normalized impedances for the 13-cell and one-cell anomalies 115

Figure 40: the three different sizes for the stomach and duodenum 120

Figure 41: the normalized impedances for the different stomach and duodenum sizes 121

IMPEDANCE MODEL FOR THE ASSESSMENT OF GASTRIC EMPTYING

I. Introduction

The original objective of this study was to investigate a noninvasive method for obtaining an image, called impedance computed tomography (ICT). The area being imaged would be a cross-sectional plane of the human body (ie. the torso or limb). When past research and our own research failed to produce accurate images, the objective was changed. The new objective would be to use ICT methods to assess gastric emptying.

Chapter II shows work done by previous researchers in the area of impedance imaging.

Chapter III deals with our own investigation into ICT. Since resolution is so poor, images were abandoned eventually in our research, and impedance methods were examined as a way to assess gastric emptying.

Chapter IV contains the conclusion. The significant results of the study are presented again, including a summary of how ICT methods can be used to assess gastric emptying.

II. Background

Section A contains a description of impedance computed tomography (or ICT): a method for obtaining cross-sectional images of the human body using low-frequency, low-amplitude currents injected into the body. This is followed by a list of biological properties of tissue and terms and definitions used in ICT studies (sections B and C). Section D presents mathematical solutions to the problem of ICT: namely, creating an image of the body's internal organs based on readings from a set of electrodes connected to a subject's abdomen. The complexity of the solution makes it necessary to use approximations.

Past approaches in applying ICT (detailed in section E) have yielded mixed results. On the negative side, ICT does not produce an accurate image. The major reasons for this are described in section F. On the positive side, ICT costs very little and presents limited danger to the patient. In addition, impedance methods do yield useful information.

With these in mind, parameters for constructing ICT systems are presented in section G. Section H contains actual prototypes that were developed and constructed. Finally a number of potential applications for ICT are presented in section I.

In summary, ICT methods show potential, with the major drawback being the low resolution of the resulting image.

A. Impedance Computed Tomography (ICT)

Impedance Computed Tomography is a non-invasive technique used to obtain a cross-sectional image of the body using a low-frequency, low-amplitude current. A set of evenly-spaced electrodes encircles the region of interest. A current source is connected across a single pair of electrodes, and the voltages across other pairs of electrodes are measured.

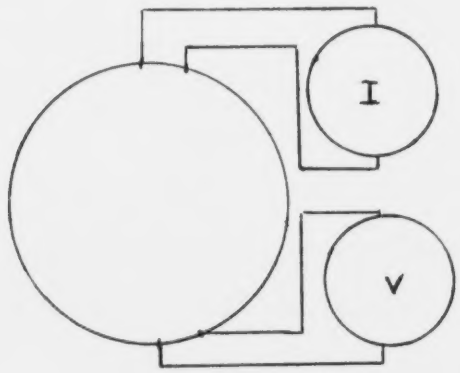

Figure 1: Basic configuration used in Impedance Computed Tomography

The current source is then reconnected across another pair of drive electrodes, and another set of voltages is measured. These values are then used to obtain a cross-sectional image of the body. Section E provides more details on the specific algorithms used to create this image.

ICT may also be referred to as 'applied potential tomography' (APT), 'electrical impedance imaging', 'conductivity imaging', and 'electrical impedance

tomography'.[1] Because of similarities between this field and the field of x-ray computed tomography, the terms impedance computed tomography (or ICT) will be used in this thesis.

There are many advantages to using ICT. Existing systems can detect impedance differences found in biological tissues. Data collection is fast, with no known hazard to the patient. Finally, the system is much lower in cost than present x-ray CT, ultrasound, and magnetic resonance systems.

The disadvantage is that the images have poor resolution. Unlike x-rays (which travel in a straight line through the body), the injected current diffuses through the body in three dimensions. It is impossible to predict either the different paths or the amount of current on each path without previously knowing the impedance distribution in the body. However, even poor resolution can yield useful information.

B. Biological Properties of Tissue

There are different ranges of resistivity in tissues. In order for these to be differentiated, impedance tomography must be able to recognize changes of at least these orders. Table 1 lists some resistivity values for

different tissues.

Table 1: A survey of published resistivity values for mammalian tissue
Source: D. C. Barber and B. H. Brown, "Applied Potential Tomography" 1984 p. 723.

This table has been removed due to copyright restrictions.

Also, special considerations must be taken into account concerning the frequency of the applied current.[2] Frequencies below 0.1 Hz will cause a periodic stinging sensation in the patient, while frequencies above 10 Hz can stimulate the nerves. Increasing the frequency beyond 10 kHz will cause a slight heating of tissue without stimulating the nerves. It is also important that resistivity can be assumed to be linear (the resistivity varies linearly with width for instance). Tissue impedance measurements at frequencies below 100 kHz show no significant nonlinearity. Thus frequencies between approximately 20 kHz and 100 kHz are safest. In addition, electric components (such as op-amps) may only operate

'properly' within a certain frequency range. This would further limit the current frequencies which can be used.

C. Terms and Definitions

Consider the situation where a single circular region with different conductivity exists in a circular region.[3] See figure 2.

Figure 2: Small conductive region embedded within large conductive region. Source: A. D. Seagar et al., "Theoretical limits to sensitivity and resolution in impedance imaging" Clinical Physiology and Physiological Measurements 1987, Vol 8 Suppl A p 13.

This figure has been removed due to copyright restrictions.

Spatial resolution is a measure of the smallest area (or pixel) to which a value of conductivity can be assigned. It is quantified as a ratio between the radius of the pixel (r_a) and the radius of the entire region (r_b).

Spatial resolution = r_a/r_b

Conductivity resolution is a measure of how accurately we can assign a value of conductivity to a pixel. If the ratio of conductivities between an object, σ_a, and its surrounding medium, σ_b, is defined to be the conductivity contrast,

$$\textbf{Conductivity contrast} = \alpha = \sigma_a/\sigma_b$$

then conductivity resolution can be quantified.

$$\textbf{Conductivity resolution} = d\alpha/\alpha$$

The quality of an image depends on both the spatial resolution and the conductivity resolution.

Noise, which is a measure of the accuracy of the voltage measurements (V), is quantified as

$$\textbf{Noise} = dV/V$$

Sensitivity quantifies the ability to detect a change in impedance in a specified area using a specified pair of voltage electrodes.[4] If a small change in impedance yields a large change in the voltages measured, the area has high sensitivity. A modified definition would be

$$\textbf{Sensitivity} = dV/dR_{(x,y,z)} = (V_p - V_0)/dR$$

where (x,y,z) specifies the area of changing impedance; V_0 and V_p, the potentials measured before and after changing the impedance by dR. If dR is just a physical constant for all (x,y,z), then sensitivity can be defined as just the change in voltages.

Gisser et al[5] introduce the concept of distinguishability. It is a measurement of how well a current pattern is able to differentiate between two conductivities (usually the actual conductivity within the body and a conjectured conductivity). It is desirable to have a high distinguishability number so that small differences will be more apparent.

D. Statement of Problem

Basically, the problem is to solve for the conductivities given the external voltages. However, the problem may be simplified if we first solve for the external voltages given the conductivities (the forward problem). Then, a reverse algorithm may be applied to solve for the conductivities given the voltages (the reverse problem).

1. Forward Problem

Initially, the problem is considered using x-ray tomography methods. In x-ray tomography, the intensity of the x-rays at the receiver is directly proportional to the sum of the densities in the x-ray path. An x-ray beam travels in a fairly straight line, losing some of its intensity each time it passes through an object. The loss in intensity is directly proportional to the density of the object. The change in intensity of the beam between source

and receiver will be directly proportional to the sum of the densities of the objects encountered on its path.

In ICT, current does not take a linear path, but instead, diffuses in three dimensions into the body. The current takes multiple paths, with most of the current travelling through the path of least resistance. The resulting voltage readings thus depends on a three-dimensional object, rather than a plane. In the forward problem, the exact paths taken by the current and the densities of currents in each path can be calculated since the conductivities are known.

The precise solution requires solving a complicated differential, so often, approximations are used. These, however, can affect the accuracy and resolution of the final image.

The following general analysis comes from Barber and Brown.[6]

The forward problem solves for the surface potentials, given the conductivities. The direct approach solves Poisson's equation for an inhomogeneous anisotropic conducting medium through which a steady current is flowing

$$\nabla (C \nabla V) = 0 \qquad (1)$$

where C is the conductivity function. The equation is nonlinear and quite difficult to solve.

If the conductivity is uniform and isotropic, then Poisson's equation can be rewritten as

$$C \nabla^2 V = 0$$

which in turn becomes the simpler Laplace equation

$$\nabla^2 V = 0 \qquad (2)$$

If the conductivity is non-uniform but isotropic (transverse conductivity equals longitudinal conductivity), then applying the outside derivative to Poisson's equation (1) yields

$$C \nabla^2 V + \nabla C \nabla V = 0$$

or $$\nabla^2 V + {}^1/_C (\nabla C \nabla V) = 0 \qquad (3)$$

or, using the log resistivity, $R = -\ln C$, then

$$\nabla R = -{}^1/_C \nabla C$$

and

$$\nabla^2 V = \nabla V \cdot \nabla R \qquad (4)$$

The solutions to these four equations solve the forward problem. There are three different classes of methods used.

Analytic methods attempt to solve Laplace's equation for the general case and then use boundary conditions to extract a single solution. Though simpler to solve than Poisson's equation, the assumption that conductivity is

uniform and isotropic affects the accuracy of the final image.

Numerical methods divide the area into finite elements (pixels) of uniform conductivity. Usually, conductivities are assigned and then the expected voltages are calculated. The conductivities are then revised after comparing the calculated voltages with the actual, measured voltages. The process is repeated for a different set of measurements until the calculated voltages match the measured ones. Numerical methods do apply to nonlinear equations. However, these methods are also iterative and can be very time consuming before any degree of accuracy is reached (ie size of pixel is small enough). Also, few methods guarantee convergence.

Approximation methods attempt to linearise Poisson's or Laplace's equation. Yamashita and Takahashi[7] claim changes in conductivity up to 30% are allowable before the linearity assumption becomes unacceptable. Since it solves a linear equation, this method is not as time-consuming as the numerical methods.

Specific approaches to both the forward and reverse problem are given in section E.

2. Reverse Problem

The reverse problem solves for conductivities (C) given the surface potentials (V). The usual approach is to find the reverse transformation for the forward problem.

In x-ray CT, the forward transformation from density of material to amount of x-rays transmitted is linear. If the different beams of x-rays are represented by a vector, c, and the densities of the medium are represented as a vector, d, then the forward transformation, T, is also an array.

$$c=Td$$

The reverse transformation is then just the inverse of T,

$$d=T^{-1}c$$

Since approximation methods are also linear, a similar approach has been attempted in ICT, with limited success. Barber et al have used a back-projection method along with some filtering (similar to the method used in x-ray CT) to obtain their images.[8]

Algebraic reconstruction provides a nonlinear solution. This is a trial-and-error method which begins with an assumption of conductivity (typically uniform) and then solves for the potentials. This assumption is then modified

using the actual measured potentials. The process is repeated until either a specified number of iterations is reached or the error drops below some defined level. The major problems with this method are that convergence is rarely guaranteed and the method is time-consuming.[9]

Past research have developed different approaches using the above methods.

E. Approaches to Impedance Imaging

1. Backprojection Methods

Linear approaches include the backprojection method used by Barber et al.[10]

In x-ray CT, the sum of the densities in the x-ray beam's path is directly proportional to the intensity of the beam as it emerges from the body. A set of parallel beams is projected through the body. It is assumed that the beams' direction does not change; each beam traveling along a straight line between source and receiver. The difference in intensity of each beam is used to calculate a valueof density. This value is assigned to all the pixels in the beam's path. Then the same set of parallel x-rays are projected through the body at a different angle. A densisty value is again calculated for each pixel and this is added to the density value from the previous sets of beams. Repeating this procedure results in a density distribution for the body plane.

In impedance tomography, the surface potential is backprojected along curved equipotential lines. The reasoning here is that the voltages depend only on the conductivities between different equipotentials (just as the x-ray intensity depends only on the densities directly in the beams path). The lines are approximated from some known conductivity pattern (usually a pattern of uniform resistivitiy). The results are then filtered to remove convolution effects.

Schomberg and Tasto also use backprojection.[11] They pass a current between a grid of small electrodes on one side of the object and a large electrode on the other side and measure voltages on the grid. Using an approximate solution to Poisson's equation, current streamlines are mapped. The resistances along the line are then integrated and a voltage is calculated. Finally, this is compared against the direct measured voltages and the differences are backprojected along the line.

Kim et al also backproject errors to arrive at the final image.[12] Measuring current densities at a grid of electrodes defines the boundary conditions; while a linearised sensitivity matrix relates change in current at an electrode to a small change in resistance of one element. Thus, by noting the voltages at the electrodes, the change in impedance can be isolated to select pixels.

All the backprojection methods assume that the equipotentials, current lines, or sensitivity of the region

changes little through an addition of a non-uniform area of resistivity (just as x-ray methods assume the beam is largely undeflected when encountering a dense object). However, since current paths do change as a result of differing impedances, backprojection will always have some error. In addition, the equipotentials are quite broad, hence blurring persists in the final image.[13]

2. Nonlinear Approaches

Others have tried the nonlinear approach (using algebraic construction) in order to increase the resolution of the image. Basically, a conductivity distribution is assumed and then successively refined using measured results.

Breckon and Pidcock[14] use direct current so that the impedance is purely resistive. They then compare the calculated voltages (using an assumed conductivity) with the measured voltages. The Newton Raphson method is then applied to the difference in voltages to develop a new pattern of conductivity. The exepected voltages are then calculated again and compared against the measured values. The Newton Raphson method is then applied to yield another conductivity distribution. the process is repeated until the error between calculated voltages and measured voltages is small enough, or until a set number of iterations have been performed. Though the method gave good results on a

model, practical implementation of the algorithm was still not available (article was published in 1987).

3. Comparing Algorithms

In most of the previous cases, each author (or set of co-authors) looked at only a single reconstruction algorithm. Yorkey and Webster[15] compare six different algorithms. These include the basic backprojection method (called the equipotential method here) developed by Barber et al and Kim et al's sensitivity matrix method (perturbation method), described previously. A third method involved recalculating the equipotential lines for each projection angle using the image that resulted from previous angles (iterative equipotential method). This is a combination of the backprojection and nonlinear approach. The fourth algorithm used Murai and Kagawa's four-electrode method based on Geselowitz's sensitivity theorem (sensitivity method). Wexler's double constraint method (whereby both the current and voltage of each element were calculated to yield its resistivity) was tested as a fifth method. The final method was developed by Yorkey himself. It used the Newton-Raphson iteration method to converge to an image which fits the measured voltages (Newton-Raphson method). The following figures come directly from Yorkey and Webster's study.

Figures 3 to 6 display the computer results using a square model and sixteen electrodes equally spaced around

its perimeter. The reconstruction was halted when the error was less than 0.01 or after twenty iterations. Though it required the most difficult computations, the Newton Raphson method converged quickest with the least error, once all the pre-computations were completed (second iteration onwards).

Figure 3: The computer model (Yorkey and Webster). Source: T. J. Yorkey and J. G. Webster "A comparison of impedance tomographic reconstruction algorithms Clinical Physiology and Physiological Measurements 1987, Vol 8 Suppl A p. 55

This figure has been removed due to copyright restrictions.

Figure 4: The error in each iteration for the six methods (Yorkey and Webster). Source: T. J. Yorkey and J. G. Webster "A comparison of impedance tomographic reconstruction algorithms Clinical Physiology and Physiological Measurements 1987, Vol 8 Suppl A p. 55

This figure has been removed due to copyright restrictions.

Figure 5: The time for one iteration of each method (Yorkey and Webster). Source: T. J. Yorkey and J. G. Webster "A comparison of impedance tomographic reconstruction algorithms Clinical Physiology and Physiological Measurements 1987, Vol 8 Suppl A p. 55

This figure has been removed due to copyright restrictions.

Figure 6: The error in the reconstructed image after one iteration (Yorkey and Webster) Source: T. J. Yorkey and J. G. Webster "A comparison of impedance tomographic reconstruction algorithms Clinical Physiology and Physiological Measurements 1987, Vol 8 Suppl A p. 55

This figure has been removed due to copyright restrictions.

F. Problems with ICT Imaging

1. Lack of Sensitivity as Distance from Electrodes Increases

A major problem with ICT methods is the lack of resolution as we progress towards the center of the region. Qualitatively, changing impedances near the surface have more of an effect on the measured potentials than changing impedances farther in the interior. Kim and Woo tried to partially offset this.[16] They adjusted the back-projected impedance of each pixel using a linear function of distance from the sensor electrode.

2. Current Travels in Three Dimensions

Another major problem was that most algorithms only dealt with a planar, two-dimensional view. In actuality, current would pass through three dimensions. Some researchers attempted to rectify this.

Jossinet and Kardous studied the distribution of sensitivity in a model using various electrode configurations.[17] The model consisted of a cylindrical conducting volume surrounded by a non-conducting medium. They found that in four-electrode systems (a current source connected across one pair of electrodes and a voltmeter connected across a different pair of electrodes), moving the voltage pair away from the current pair increased the sensitivity of interior points (ie. small changes in impedances near the center of the torso are more easily

detected in the voltage electrodes when the voltmeter is connected across electrodes farther from the current electrodes). This also created a more even sensitivity distribution. The change in surface potentials depends less on the location of the impedance changes.

However, this configuration resulted in null lines appearing between source and pickup electrodes. Near these lines, the sensitivity decreases to zero.

Also, they found that the sensitivity outside the two-dimensional plane is not negligible. In fact sensitivity was affected by objects within a vertical dimension to the same order of magnitude as the diameter of the model.

Another approach to this problem involves the use of guard electrodes to limit the current paths to one plane.[18] The current input electrode is surrounded with a guard electrode (a circular plate electrode with an opening in the center) set at a potential which minimised the radial potential gradient from the current input electrode.

However, Plonsey and Collin have shown that a change in resistivity can cause either an increase of decrease in the overall impedance seen at the (guarded) electrodes.[19] This is more significant when the area of changing impedance is closer to the electrodes; specifically in the region between the current drive and voltage measurement electrodes. In fact, Smith has shown that increasing resistivity outside the plane may show up as a decrease in impedance at the voltage electrodes.[20]

3. Shape of Individuals must be Considered

A general problem with ICT is that the shape of the body must be recorded. Current pahts and equipotentials (and hence the resulting image) are affected by the shape. Smith describes an apparatus which can record the shape of the body as well as take voltage measurements.[21] A diagram of the apparatus is presented in figure 7.

Figure 7: Electrode carrier for CT-Imaging showing the Effective Measurement Zones Source: D. N. Smith, "Determination of impedances using numerous simultaneous currents (DINSC) - system design and practical applicatons" University of Edinburgh an Lothian Health Board UK p 69.

This figure has been removed due to copyright restrictions.

Another method of circumventing the shape problem is the linear array described by Powell, Barber and Freeston.[22] Electrodes are attached to a small flat surface which is handheld against the body surface of interest. The current density introduced in the body is higher near the array than farther from the array. Thus the result is an image of a

smaller region next to the electrodes, rather than a planar cross-section through the entire body.

The method has some advantages over the encircling model. Since the electrode configuration is known, the amount of calculation is reduced. Also, the image has finer resolution than an encircling array due to the smaller area. The array is mobile and flexible in that interchanging probes of different dimensions easily alters the resolution.

Results using a 1mA, 50kHz displacement current are shown in figure 8. Backprojection was used as a reverse algorithm.

Figure 8: Image of simple back-projection of the change in resistivity between inhalation and exhalation Source: H. M. Powell et al., "Impedance imaging using a linear electrode array" University of Sheffield p 90.

This figure has been removed due to copyright restrictions.

The voltage read is compared with the voltage expected from a uniform distribution, and the resulting ratio is used to estimate resistivity for the region. Using sensitivity

studies, changes in conductivity at depths of up to half the array length can be detected.

The major problem with the linear array method though is that the electrodes show little sensitivity as the distance from the surface is increased. This is shown in the graph of figure 9.

Figure 9: Graph of peak image amplitude against distance of point from array Source: H. M. Powell et al., "Impedance imaging using a linear electrode array" University of Sheffield p 90.

This figure has been removed due to copyright restrictions.

Despite these problems, Impedance imaging techniques can still be used in selected situations. For instance, they can be used to detect changes in impedances near the surface of the skin, especially when the shape and conductivity distribution can be well-estimated. Some applications are documented in section H.

G. Physical Factors in Constructing ICT Systems

The previous section dealt with the theoretical problems of ICT. In this section, the physical aspects associated with putting together an impedance measuring system are described. Unfortunately almost all of the systems are proposed only or set up to work on a model rather than the human body. Clinical applications are still forthcoming.

1. Number of Measurements and Data Collection Times

First, the number of measurements must be established.[23] Using N electrodes, there are N pairs of adjacent current source electrodes. For each pair of current electrodes, there are N-1 pairs of adjacent voltage measurement electrodes. Deleting configurations which switch current electrodes for voltage electrodes yields a total of N(N-1)/2 measurements. The reciprocity law shows that switching current-drive and voltage-measurement electrodes would yield the same measurements. The voltage profiles for the cases when the current source is connected to any non-adjacent pair can be obtained using superposition.

Data may be collected in parallel if (N-1) amplifiers are available. The minimum collection time is thus N/f, where f is the frequency of the current source. Thus, for

16 electrodes, and a frequency of 20 kHz, data collection time is 0.8 ms, well within most biological cycles.

2. Electrode Impedance and Capacitance

A common problem with all methods involves the electrodes.[24] Electrodes act as transducers and cannot be ignored in two-electrode systems (ie current is driven through the same pair of electrodes that potential is measured across). Barber and Brown suggest using four electrodes with the current applied between the outer two electrodes and the potential measured within the inner pair. However, in this system, capacitance between current drive and voltage electrodes can create an unwanted current path. Similar considerations would be necessary should guard electrodes be used.

3. Current Source

Using current sources with a single fixed frequency (or even direct current) pose few problems. However, significant advantages arise from using variable currents.

Griffiths and Ahmed discuss the application of two currents of different frequency to the body.[25] Since the resistance of different tissues differs at different frequencies, the two resulting images can be compared to note changes in only specific tissues.

A study by Gisser et al indicates that the (source) current should not be a simple trigonometric function at

all.[26] They define the best currents as the set of currents which maximizes the distinguishability between two known conductivity distributions. This is handy in the event we are trying to isolate changes in specific areas of the body. Here a conjectured conductivity for the body can be modified slightly (in one region) to produce the second conductivity pattern.

The best currents are mathematically shown to be the eigenfunctions with the largest eigenvalue of a linear operator. The paper presents an example of the method used to mathematically derive the best currents given two known conductivity distributions.

The paper also presents a successive approximation approach to yield a sample set of best currents without a priori knowledge of the conductivity pattern inside the body. First estimate the conductivity pattern expected. This is the reference pattern. Then estimate a current. Apply this current to the body and compare the voltages measured with the voltages expected when the current is applied to the reference conductivity. Divide the voltage differences by their mean to arrive at a new current estimate. Repeat the procedure until the new current estimate differs from the previous current estimate by an acceptable value. Unfortunately, there are presently no publications which show the images that would result when a set of best currents is used.

Should the above ideas be implemented, ICT systems may involve design work on the current sources.

H. ICT Prototype Systems

1. Kim and Woo's Prototype System

Kim and Woo have designed a prototype system to obtain images from circular models.[27] A functional block diagram is shown in figure 10. The host computer is an Intel 380 microcomputer using an Intel 80286 microprocessor ,an Intel 80287 Numeric Data processor, and an Intel 80186 graphics display processor. Though it is possible to process the image on the host computer, a modem accesses an IBM 4341 computer for faster reconstructions.

Figure 10: The functional block diagram of the overall impedance imaging system Source: Y. Kim and H. Woo "A prototype system and reconstruction algorithms for electrical impedance technique in medical body imaging" Clinical Physiology and Physiological Measurements 1987 Vol 8 Suppl A p 39.

This figure has been removed due to copyright restrictions.

The system is versatile. Each electrode's function is governed by its own analog switch, allowing it to do one of the following: (1) apply voltage to the object, (2) measure current, (3) be grounded, or (4) logically disconnect from the object. Furthermore each electrode is connected to a multiplying digital-to-analog converter (capable of 256 discrete levels) which controls the applied voltage.

A modified sensitivity algorithm is used to reconstruct the image. The logarithm of the sensitivity values were used and the region is divided into columns of elements, pointing in the direction of expected current flow, for each sensor. This reduced scope method removes reconstruction steps based upon redundant data. The result is a faster (though not improved) final image.

The results of the simulation study are as expected. As an element's size increases, or its distance to the sensor decreases, the higher its sensitivity. Sensitivity is also increased when the background resistivity is decreased. Some modification in the algorithm is provided to partially offset these effects.

A 100kHz voltage was applied across one pair of sixteen (pairs) of electrodes. Eight equally spaced electrodes were used (exactly one quarter of the total circumference) as source electrodes while the currents at the opposite eight electrodes were measured. The model consisted of a glass container filled with agar. The incongruous elements were represented by square blocks cut out of the agar solution.

The final image is fairly accurate, with most of the error occuring around the edges of the elements. In a way, these represent the best solutions possible, as the difference in resistivities between air and agar is much higher than the differences between bone and tissue.

2. Barber and Brown's Prototype

Then, there is the working imaging system designed by Barber and Brown.[28] A block diagram is shown in figure 11. Data collection is fast. Each measurement can be taken inside 1 ms. With sixteen electrodes, one data set (providing one image) can be taken in 100 ms (data is taken serially). The method takes the voltage measured divided by the voltage expected in a uniform-conductivity model and then backprojects the logarithm of this ratio between equipotentials ending on that electrode pair. In addition, electrode effects are not considered. A result is shown in figure 12. Even Barber and Brown admit that the image has low spatial resolution.

Future systems will concentrate on decreasing noise effects, increasing image resolution, and improving the efficiency of reconstruction algorithms and data acquisition methods.

Figure 11: Block diagram showing electrodes around a body and multiplexing electronics Source: B. H. Brown et al "Applied Potential Tomography: possible clinical applications" Clinical Physiology and Physiological Measurements 1987 Vol 8 Suppl A p 110.

This figure has been removed due to copyright restrictions.

Figure 12: A resistivity cross section of an arm Source: B. H. Brown et al "Applied Potential Tomography: possible clinical applications" Clinical Physiology and Physiological Measurements 1987 Vol 8 Suppl A p 110.

This figure has been removed due to copyright restrictions.

I. Applications of ICT

Even though few working systems have been implemented, ICT shows potential. There are applications for ICT in a number of areas. A number of these are summarised by Barber and Brown.[29]

In plethysmography, once the relation between changes in volume and changes in impedance is identified, ICT can be used to diagram the cardiac cycle. ICT should be capable of detecting 0.1% impedance changes with a spatial resolution of 10 mm when applied to an arm of diameter 8 cm. See figures 13 and 14.

Figure 13: An applied potential tomographic image of a forearm constructed from a 16-electrode circular array Source: B. H. Brown et al "Applied Potential Tomography: possible clinical applications" Clinical Physiology and Physiological Measurements 1987 Vol 8 Suppl A p 110.

This figure has been removed due to copyright restrictions.

Figure 14: Diagrammatic cross section of the forearm Source: B. H. Brown et al "Applied Potential Tomography: possible clinical applications" Clinical Physiology and Physiological Measurements 1987 Vol 8 Suppl A p 110.

This figure has been removed due to copyright restrictions.

ICT can also be used to identify gastric contents. Present images suggest that fluid changes of the order of 10 ml should be measurable. However, this may be erroneous, in that both the volume and resistivity of the stomach contents can change simultaneously. Both affect the voltages measured. A change in pH will also change the contents' resistivity. A proper imaging system must be able to separate the effects of a changing volume from those of a changing pH.

In impedance pneumography, sixteen electrodes would allow the detection of separate impedance changes between both lungs. Since lung tissue has a high resistivity (as

compared to the stomach), the presence of any fluid within them should result in a very noticeable drop in resistivity.

ICT can also be used to detect intraventricular haemorrhage. At present, ultrasound detects intraventricular bleeding in premature babies. However the method is technically difficult and not good for continuous monitoring. Placing electrodes on the head is more accessible and safer for the patient. There is even literature which predicts the voltage profiles within the brain when a current is applied.

In the area of athletics, ICT can be used to measure lean-fat ratios in the body. Fat resistivity is approximately five times larger than muscle resistivity. ICT easily resolves differences of less than 1.3 times.

An interesting use for ICT is in hyperthermia treatment for cancer. Griffiths and Ahmed (and before them, Conway et al) explore this possibility. The objective is to obtain a thermal distribution image of tissue. What is required is some characteristic which directly relates to temperature and can be easily measured. Conductivity for tissue changes 2% for each one-degree change in temperature (typical for muscle tissue). This is much higher than the x-ray attenuation coefficient of 0.04% per one-degree change in temperature (the corresponding value when using x-ray computed tomography).

Finally, ICT can be used for detecting tumors. It is expected that the highly vacularised tissue surrounding

tumors have a low resistivity in contrast to an avascular core. X-ray techniques presently have limited success, and fluid-filled cavities give poorly defined ultrasound pictures.

J. Summary

As the above applications show, ICT has a lot of potential. Faster computers and more accurate measuring devices should improve the reliability of the results. Its largest drawback is in the accuracy of the image that results. In all the applications, some characteristic (for instance, air volume in the lungs) changes with impedance or depends on the impedance. The more accurate the image (and hence the impedances along the cross-sectional plane), the stronger the conclusion which can be drawn from the image.

Also, in some applications, high resolution is not required. Here, the advantages of ICT outweigh the disadvantages. Or in some cases, ICT can be used as an initial method of measurement (thereby determining whether a more accurate, but more potentially dangerous method, is required). The central theme is that functional information may be acquired despite the poor resolution.

This is the approach which has been adopted in our own research. It is undesirable to develop conlusions from an inaccurate image. Instead, the impedances which are measured using ICT methods will be considered instead. It will be shown that these values can be used to assess

gastric emptying.

III. Experimentation

This chapter contains the details of the experiments. Four planar models were developed for this study. The initial model was the square-resistor array model. This was then modified to create the circular array model. Though very similar to the first model, the second model used fewer cells and hence decreased the number of computations required. It could still be adaptable to most abdomen shapes. The third model was a computer simulation of the first and second model. Though it posed its own problems, the working program now allowed experiments at a fraction of the previous time. It was capable of calculating the equivalent impedance between any two points in the model. Finally, the electrolytic model was developed to represent a continuous distribution of resistivities. It provided a check against the results from the three previous discrete models.

A. The Square Resistor-Array Model

1. Purpose

Most of the previous research divided the plane of interest into a set of finite elements. Then, using various assumptions, a reverse algorithm was developed. For instance, in Barber and Brown's work, current paths (and hence equipotentials) varied only slightly. The voltages

measured between a pair of equipotentials was assumed to depend only upon the resistivities between the two equipotential lines.

Previous approaches required two different approximations. Firstly, a finite-element model approximated the continuous impedances found in the human body. Secondly, other assumptions were required to solve either the Laplace or Poisson's equation.

A different approach was attempted in these experiments to decrease the number of approximations. Instead of using finite pixels as cells, this model used resistors on the edges to form cells. Hence instead of a 'solid' square of uniform resistivity, our model used a square formed by four resistors, each of which could have its own value of resistance.

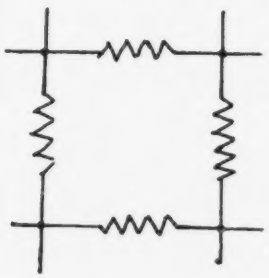

Figure 15: Single cell of the square resistor array model

It is reasonable to assume that as the cells are made smaller and smaller, that this model can approach a continuous state just as in the finite-element approach. Unlike previous methods though, this model could be solved

precisely using Kirchoff's voltage laws or Kirchoff's current laws.

Secondly, this array could represent any shape. This can be accomplished using two methods. The first method entails physically removing cells to obtain the desired shape. The second method involves replacing some of the resistors on the edge of the array with much higher impedance values. Both methods are used in the study.

There were other advantages as well. The model could be extrapolated to three dimensions fairly easily. Kirchoff's laws would still apply. The problem was now more computationally-intensive, but not more difficult. Different resistivities were achieved by changing the resistances of the cells in question. To simplify computations, the model was built only in two dimensions.

2. Description of Model

Initially, this model would simulate a very simple situation: a square torso containing material of uniform resistivity. One or two items of higher resistivity (anomalies) would be placed within the torso (to represent bone for example). Though very simplistic, the intent was to determine a) whether the anomaly could be detected, and b) whether its location could be discerned.

This model consisted of four hundred cells (a twenty-by-twenty array). By judiciously choosing certain edge resistors to have infinite resistance and others to have

zero resistance, the model could effectively simulate any torso shape desired. Initially, 100-ohm resistors were used throughout the board. To represent anomalies, certain resistors were removed and either replaced with resistors of 1 M ohm, or simply not replaced at all. An impedance meter (Hewlett Packard Multimeter, model 3490A) was connected across pairs of nodes on the edge of the array.

3. Experiments

Initial experiments used single-cell anomalies (or holes) at different locations on the grid. Three different locations were chosen, and for each of these, four separate sets of impedance measurements were taken. Each of these sets were compared in turn to the set of impedance measurements obtained when no anomaly was present. The differences in measurements were then examined to determine whether the anomaly could be detected, and if so, whether its location could be discerned. The differences were examined in a number of ways. Details of the experiment follows.

First, though, there should be some clarification of the terms used in the apparatus description. The first line identifies the model used in the experiment. The next two lines detail the values of the resistors used in the model: first, the resistances of the anomalies, followed by the resistances used in the rest of the array. The fourth line identifies the electrode (probe) locations. The impedance

electrodes are located on the outside edges of the array (to represent the surface of the torso). Any additional lines detail other equipment used in the experiment.

Experiment 1: IMPEDANCES OF SINGLE-CELL ANOMALIES

OBJECT:

Since the impedance of air is much higher than internal structures (such as tissue or bone), this experiment will show the maximum variations in surface measurements that can be expected.

APPARATUS:

Square Resistor Board Model
Anomaly resistors = open circuit
Normal resistors = 100 ohms
Probes are on the surface
Hewlett Packard 3490A Multimeter

PROCEDURE:

The resistors that comprise a single cell are removed from the resistor board. Then, using the multimeter, the impedances are measured across diametrically opposite nodes in four methods. All the nodes are on the outside edges of the array. In row measurements, the impedance meter is connected at two points along the same row of resistors. There are twenty-one rows of resistors in the array, and hence twenty-one measurements. In column measurements, the two points are on opposite points along the same column. The final two sets of measurements are diagonal measurements (at 45 degrees to the edges). There are the diagonals connecting the left-top corners to the bottom-right corners

(left-top diagonals) and the diagonals connecting the right-top corners to the bottom-left corners (right-top diagonals).

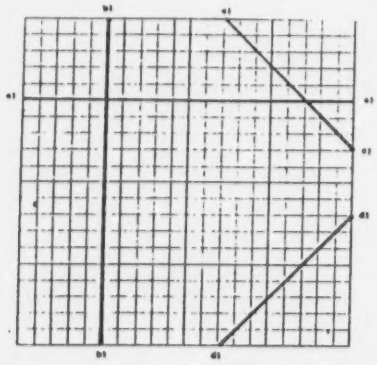

Figure 16: A sample a) row, b) column, c) left-top diagonal, and d) right-top diagonal in the square resistor array model

Three different locations were chosen for the single cell: the cell at row 5 column 17 (R5C17), row 10 column 10 (R10C10), row 12 column 19 (R12C19). See figure 17. Results of these and the situation when no cell was missing (uniform resistivity with no anomaly) were graphed.

RESULTS:

Figure 18 is a graph of the impedances measured. The impedances vary from approximately 0.39 k ohms to 0.08 k ohms (approximately 80% to 400% the impedance of a single resistor in the other parts of the array). The resistors can err up to five percent (an error of .005 k ohms). The general shape of the row and column graphs are the same, which is to be expected since the array is symmetrical. The same applies for the two diagonal graphs. However, the two

graphs are not exactly the same showing the anomaly is detectable. As the anomaly moves closer to the center of the array, it becomes harder to detect.

However, while the anomaly is detectable, it's location is more difficult to assess. It was hoped that the row, column or diagonal which intersects the missing cell would show the largest deviation (from the measurements when no cell was missing). Unfortunately, that is not the situation. The greatest deviation occurs when the anomaly is placed at R12C19.

Figure 18 shows a graph of the difference in impedances between the single-cell anomaly situation and the situation when there is no anomaly. The differences are most noticeable in the R12C19 case, but even these results show a maximum difference of less than four times the error value (5 ohms). Again, the row (or column or diagonal) which shows the maximum difference does not coincide with the row which contains the anomaly.

Figure 20 shows the results after normalizing the diagonal measurements. The impedance differences are divided by the number of cells in each diagonal. The intention was to remove bias that may result due to the number of resistors along the diagonal. Still, the largest impedance does not coincide with the row, column or diagonal which intersects that cell.

A further attempt was made to emphasize the differences. At this point, detecting the differences was

more important than locating the anomalies. The anomaly measurments were divided by the no-anomaly measurements in hopes of isolating significant differences. (For example a difference of +2 ohms when the norm is 6 ohms shows the same percentage increase as a difference of +4 ohms when the norm is 12 ohms). It was hoped the ratio of impedances might yield better results. The R10C10 values were now less than the R5C17 values in all cases. This agrees with the expectation that anomalies closer to the center of the torso are harder to detect than anomalies closer to the outer surface.

A final strategy to determine the anomaly's location was attempted. If column, row and diagonal measurements couldn't isolate the cell by themselves, perhaps their combined total would yield better results. (Much like x-ray computed tomography, where the resistivity of a single pixel is determined using a number of different measurements, rather than just one.) Thus, the measurements for the row, column and diagonals which bisected each cell were summed in the R5C17 situation.

On the graph, it would be difficult to label the x-axis using the row-column method previously outlined. For convenience, each cell was identified with a number between 1 and 400. Row 1 contained cells 1 to 20, row 2 contained cells 21 to 40, and so on. The anomaly was located at cell 97. When the results were graphed in figure 21, a periodic waveform was the result. The values for cell 97 were not

distinct from the rest, so once again, the location of the anomaly could not be determined.

SUMMARY:

In conclusion, a single-cell anomaly is detectable, when compared against a situation with no anomalies. However, the difference is small, less than four times the error value of a single resistor. Its location was also difficult to assess based on these measurements. As the anomaly approached the edge (away from the center) of the array, it had a higher difference in impedance.

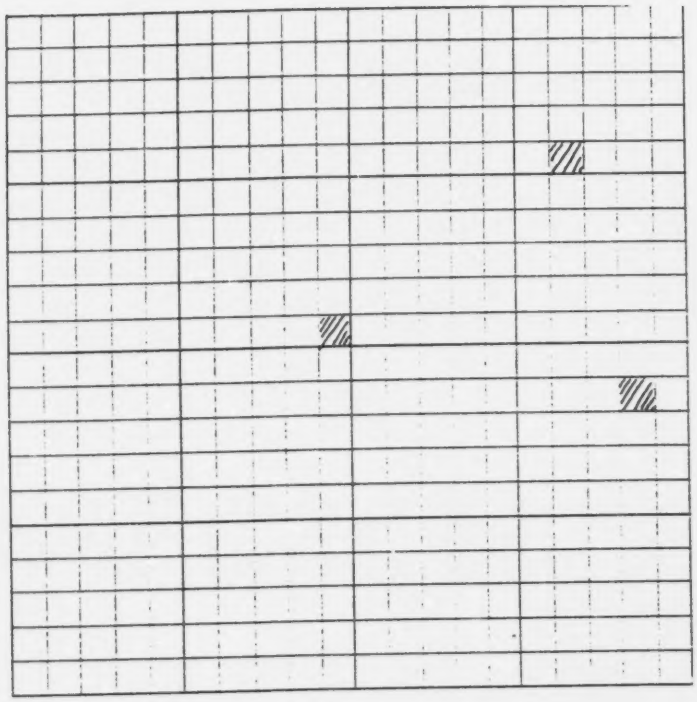

Figure 17: Locations of the single-cell anomaly in the square resistor array model

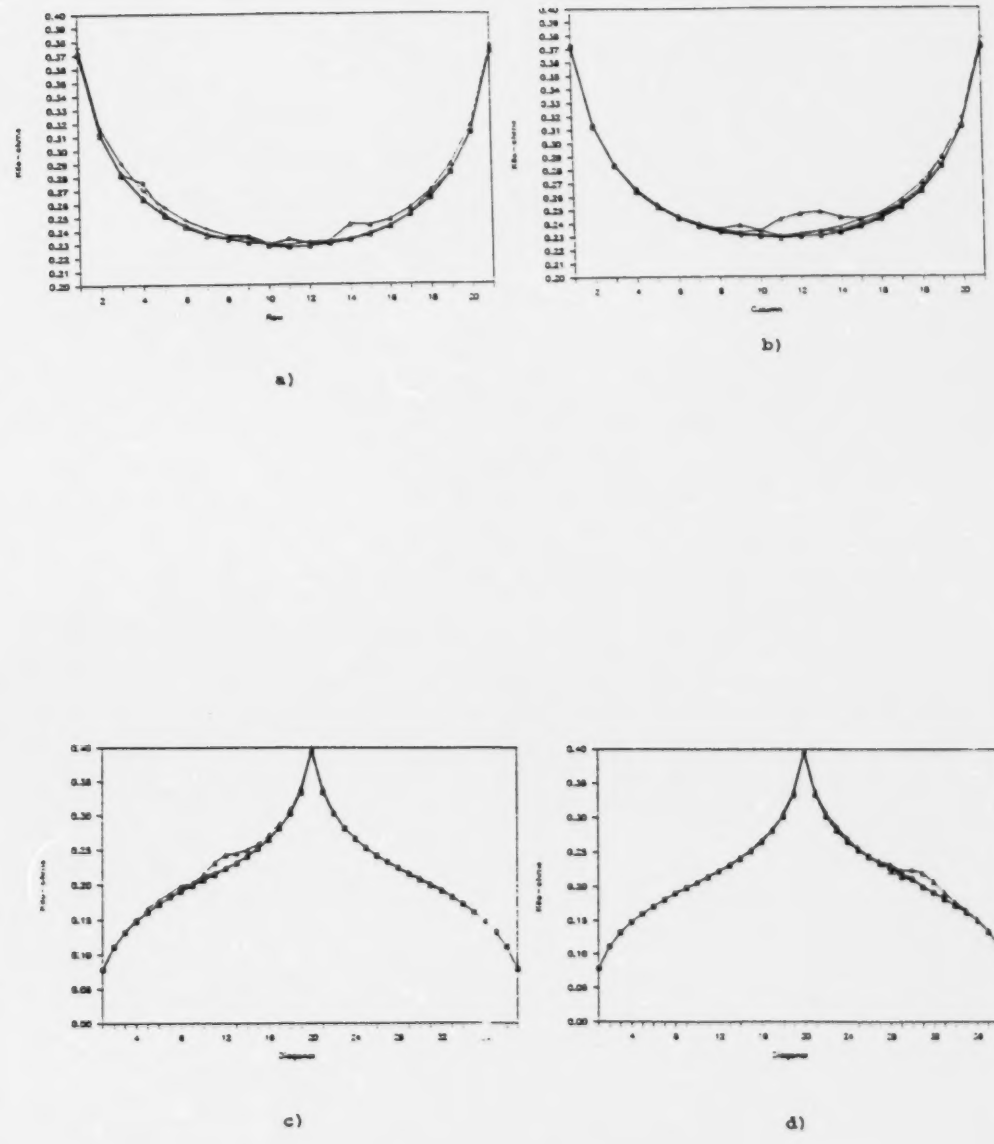

Figure 18: Impedances of a) rows, b) columns, c) left-top diagonals and d) right-top diagonals in the square resistor array □ None missing + R5C17 ◊ R10C10 △ R12C19

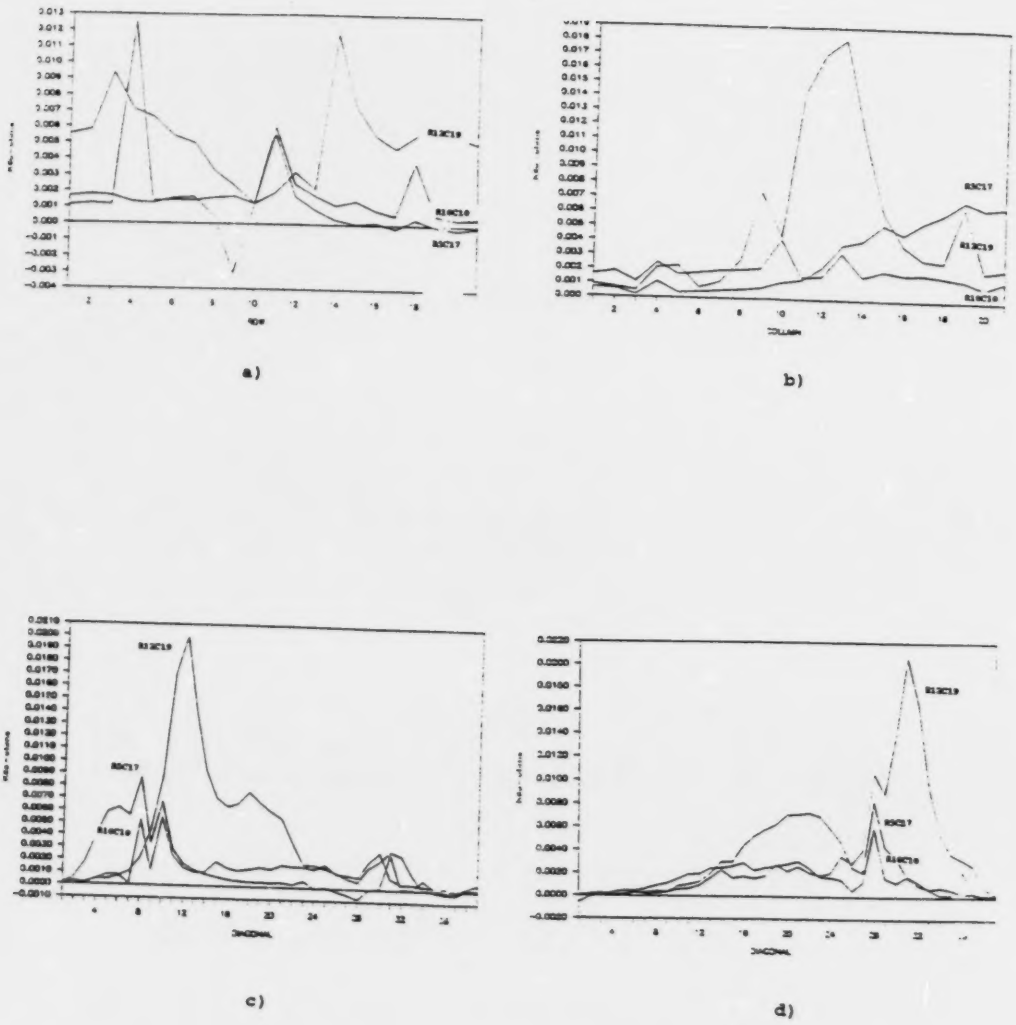

Figure 19: Differences in impedances measured between single-cell anomalies and no anomaly a) rows, b) columns, c) left-top diagonals, and d) right-top diagonals

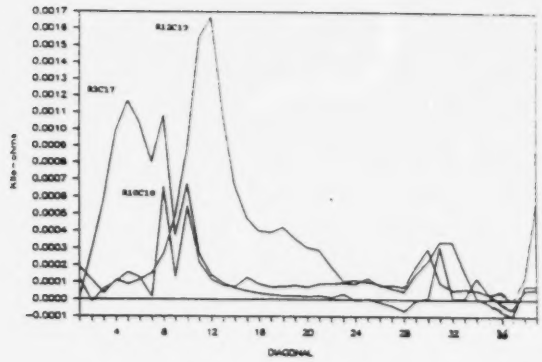

a)

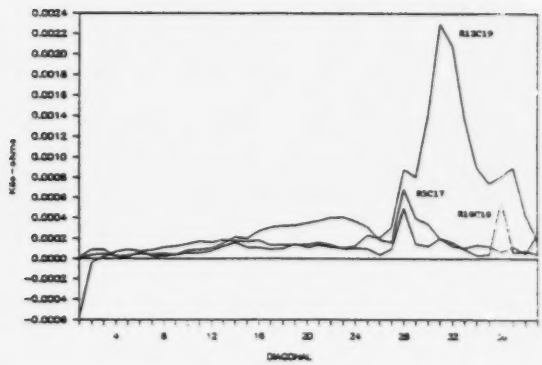

b)

Figure 20: Difference in impedances measured divided by the number of cells in the diagonal for a) left-top diagonals and b) right-top diagonals

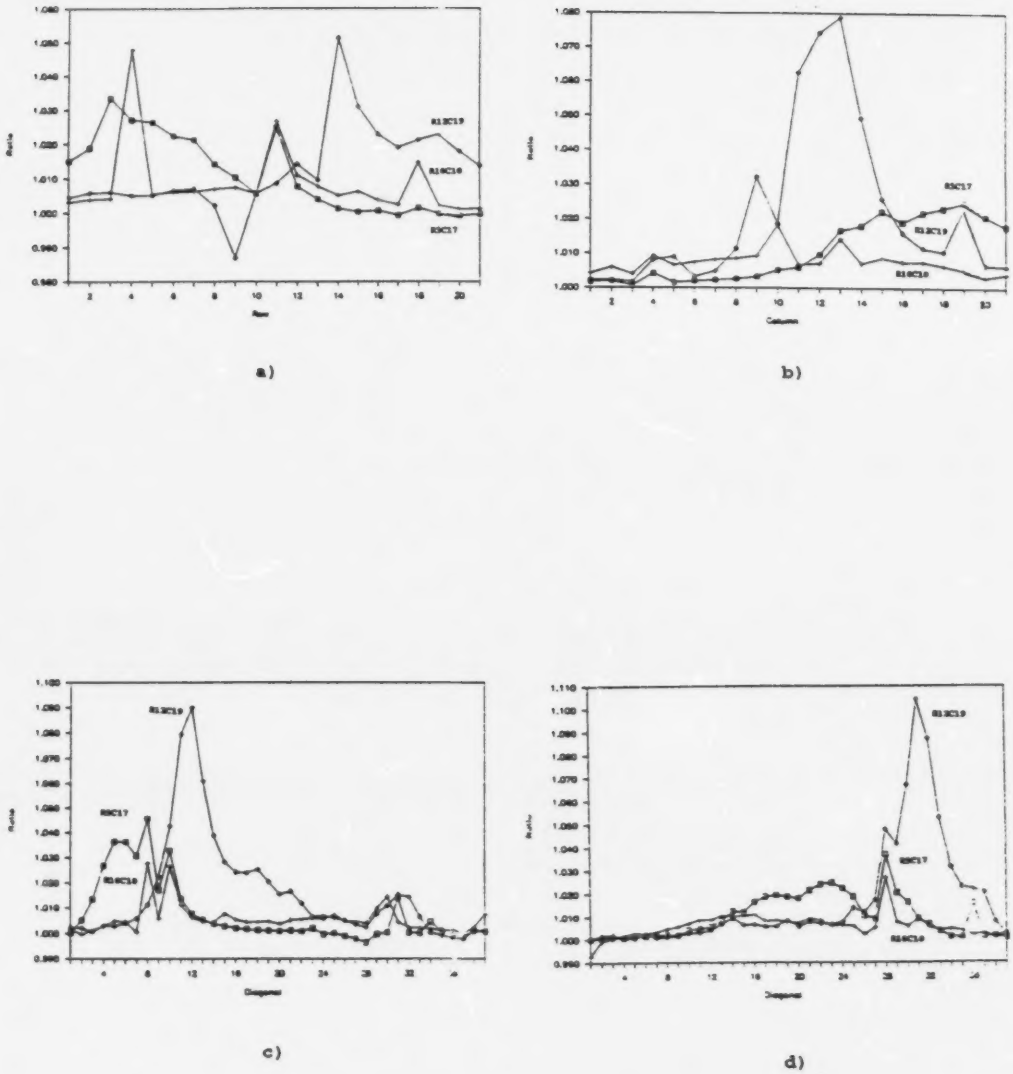

Figure 21: Normalized impedances of a) rows, b) columns, c) left-top diagonals, and d) right-top diagonals

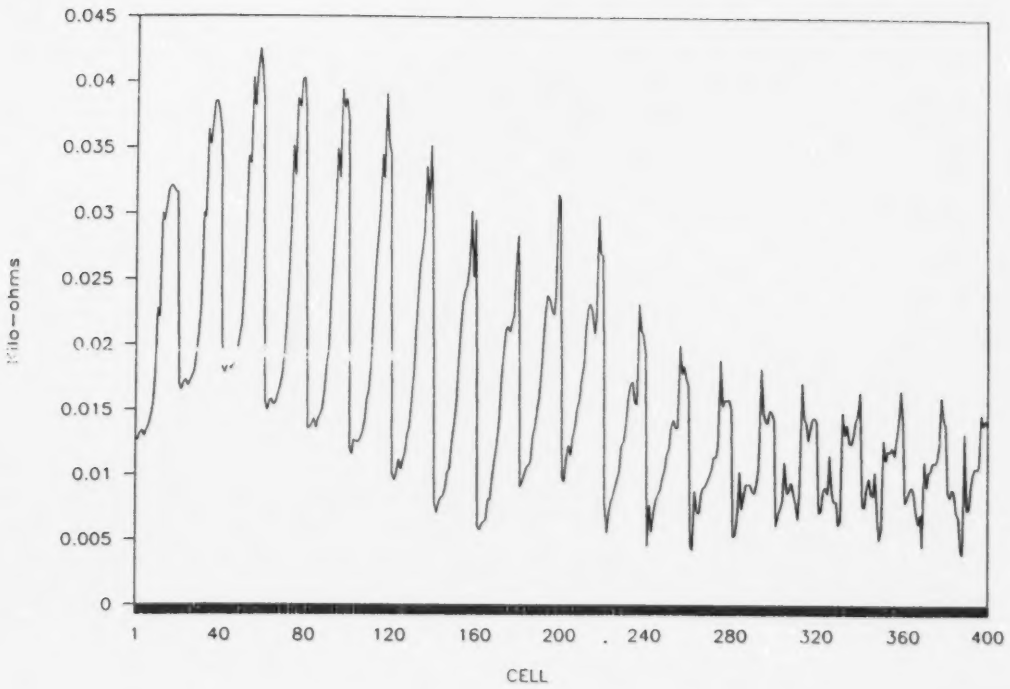

Figure 22: Total differences in impedances for the configuration with the R5C17 anomaly

4. Model Summary

Results from the square resistor array showed that single-cell anomalies were barely detectable, and their location could not be determined. Anomalies closer to the surface had a larger effect on the impedance measurements. Clearly, the model would need modification.

B. The Circular Resistor Array Model

1.Purpose

The results from the square resistor array model were less than promising. One of the problems was the excess resistors on the corners of the array. Since this placed a good portion of the array edges farther away from the anomaly, it was decided to modify the array to have a more circular shape. Also, the new configuration would more accurately resemble the human torso.

This model still maintained the advantages of the previous model. The circular array could still represent any shape by setting the appropriate resistor values to high values and others to zero. This model could be solved accurately using Kirchoff's laws.

At this point, the goal of the experiments was still to detect and locate anomalies.

2.Description of Model

Certain cells were removed from the edges and a circular shape was the result (figure 23).

A new method for selecting opposite nodes was determined. Rather than specifying rows and columns, the impedances were measured directly across diagonals this time. Each diagonal connected across the center of the array, effectively bisecting the array into two circular halves. The first diagonal started at the top-left 'corner'

of the array (figure 23). Subsequent diagonals were numbered in a clockwise direction, each new diagonal separated from the previous one by one row or one column.

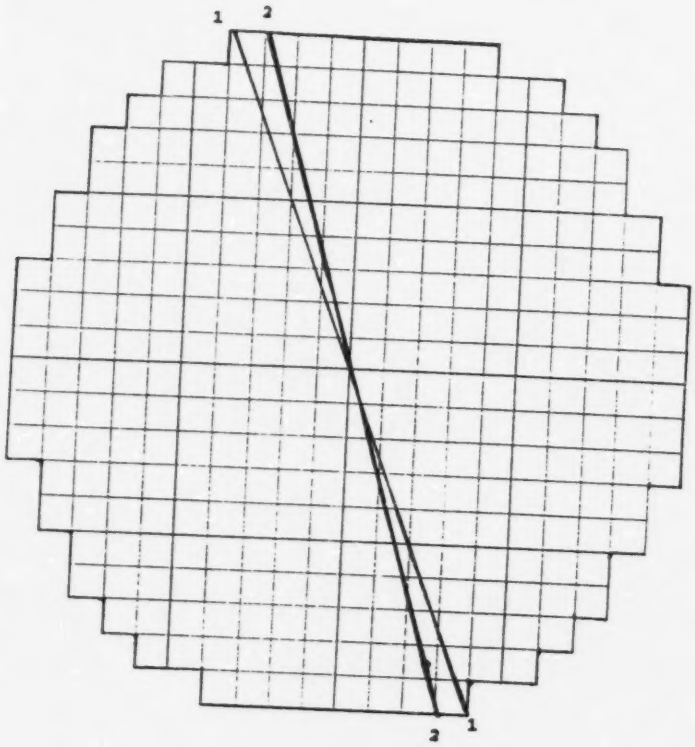

Figure 23: Configuration of the circular resistor array model with diagonals 1 and 2 indicated

3. Experiments

The initial experiment used the same anomalies as the ones used in the previous experiment (ie. R5C17, R10C10, and R12C19). The objective was to determine whether an anomaly

could be detected, and if so, whether its location could be discerned.

The goal of the second experiment was to assess the current deflection caused by two anomalies. When a current encounters an object of high impedance in its path, the current will diverge around it. The question is, would significant current lines be diverted far enough away from the anomaly to be detectable at the surface?

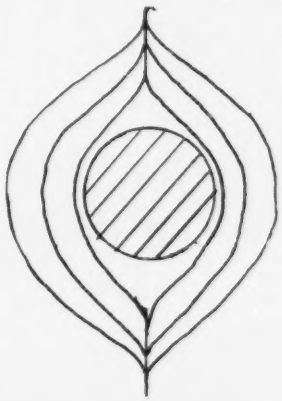

Figure 24: Current path lines diverging around an object of high impedance (continuous medium)

A current source was connected across a diagonal and the voltages were measured across each individual resistor in the array. With the exception of the resistors in the anomalies, all other resistors had the same value of 100 ohms. Hence current and voltages were directly related, and the resistors with the largest potential differences also had the highest current.

Experiment 2: IMPEDANCE MEASUREMENTS ON A CIRCULAR ARRAY

OBJECT:

The extra resistors on the square array allowed currents alternate paths to diverge into. Also, the edge of the array was further away from the anomalies. This experiment improves on the model by allowing fewer paths and by bringing the edges closer to the anomalies.

The objective is still to determine whether the anomalies can be detected using surface measurements.

APPARATUS:

Resistor Board Model (circular)
Anomaly resistors = open circuit
Normal resistors = 100 ohms
Probes are on the surface
Hewlett Packard 3490A Multimeter

PROCEDURE:

Using the same four anomalies of experiment one, impedances across diagonals were measured. Unlike the diagonals of experiment one, these diagonals effectively bisected the array.

RESULTS:

Differeneces between the single-anomaly case and the norm were much higher using the circular array, as compared

to the square one. In the R12C19 case, the difference reached over 1 k ohm in diagonals 26 and 27.

The impedance difference for the R5C17 case was also more pronounced than in the square resistor case. This is probably due to its new location, one much closer to the edge of the array.

The impedance for R10C10 reached maximums at diagonals 5 and 24. At this time, there is no explanation as to why there are sudden increases in the impedances measured. (Later, it was determined that this was due to the shape of the array. The model was not perfectly circular. Steps were taken to resolve this problem. See section E.)

The measurements are fairly symmetrical as expected, even though the array is not perfectly round.

When these key diagonals are plotted in figure 26, the diagonals also define the angle of the anomaly (except in the case of the central anomaly).

Finally, the amplitude of the impedance differences suggest that the approximate radial distance of the anomaly (from the center) may be determined. More experimentation is required. (see section C.)

SUMMARY:

Diagonal measurements across the circular array yielded much better results than the measurements used in the square array. Firstly, the impedance differences are much larger than the error value for the resistors. Secondly, the

diagonal along which the anomaly is situated coincides very closely with the diagonals of highest impedance.

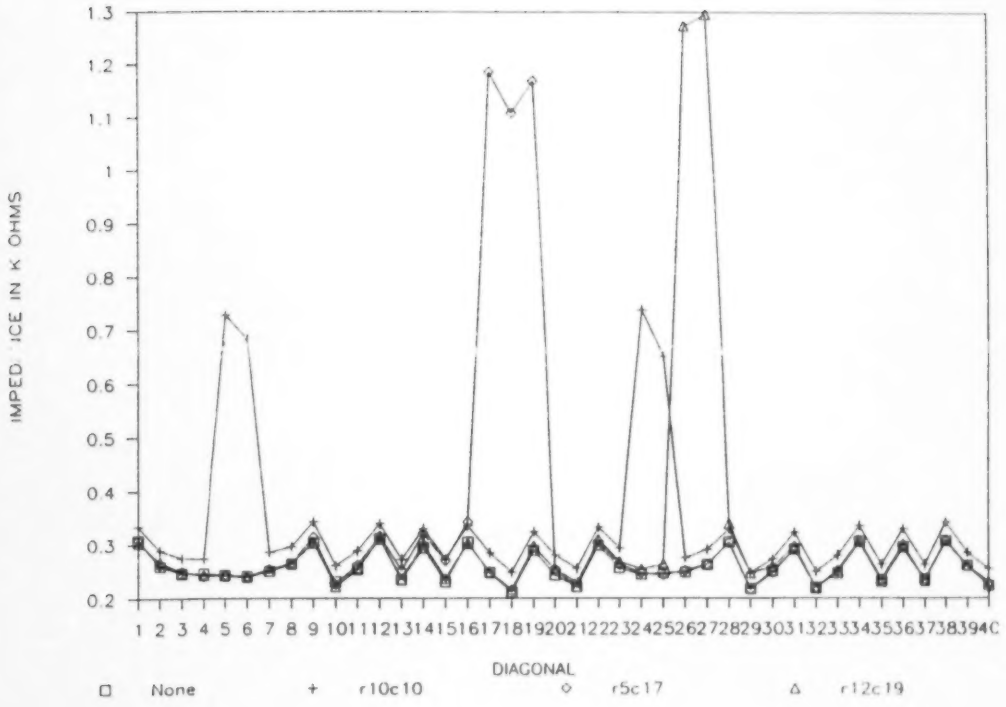

Figure 25: Impedance measurements for the circular resistor array model

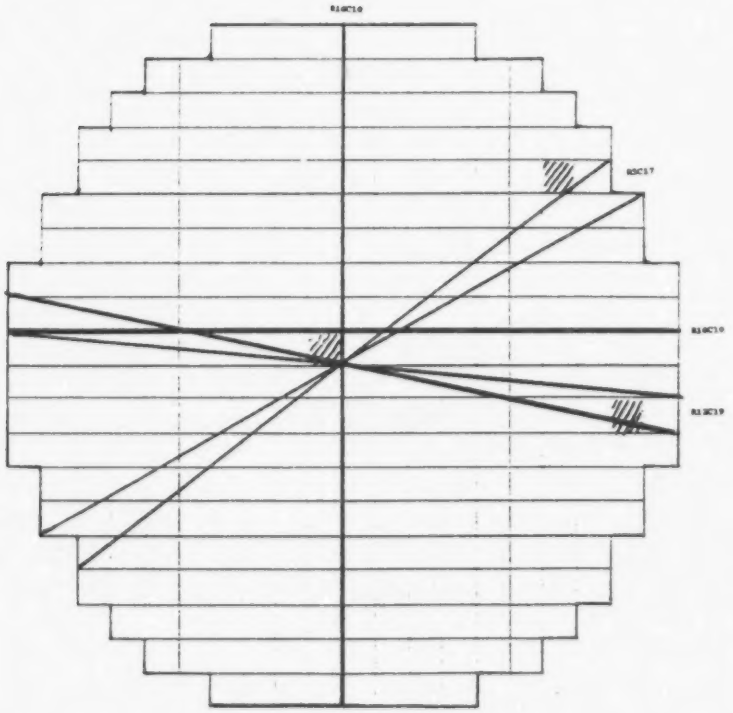

Figure 26: The diagonals which had the highest impedances measured for each anomaly

Experiment 3: VOLTAGE DENSITIES WITH ANOMALIES

OBJECT:

Previous experiments showed impedances could be detected but could not explain why there were extreme increases in the impedances measured at specific diagonals. In addition, other research have measured voltages across different pairs of locations on the surface. Since the resistances were known, the currents could be determined by measuring the voltages across each resistor. To investigate the deflection of current in the array, the following experiment was conducted.

When an anomaly is placed within the environment (by replacing the resistors that form a block with higher values), current will flow around the anomaly (the current taking the paths of least resistance). It was desired to note if the current paths diverged enough to affect the surface readings.

APPARATUS:

Circular Resistor Board Model
Anomaly resistors = 100 k ohms
Normal resistors = 100 ohms
Hewlett Packard 3490A Multimeter

PROCEDURE:

Two anomalies were placed in the model. One was a one-by-one cell at row 13 column 14. The other was a three-by-

three block centered at row 17 column 6. Two anomalies were used to better define the current paths (It was hoped that the anomalies would create enough current divergence so that the two anomalies would effectively act as one large anomaly, and a large percentage of the current would diverge around both anomalies).

The current source was connected to the top-left corner of the cell at row 4 column 3 and to the bottom right corner of the cell at row 17 column 18.

RESULTS:

The highest current densities occurred in the resistances closest to the current sources. Densities were lower near the center of the resistor array. Current densities around the anomalies fell sharply (greatest effect at a radius of one cell from the anomalies but very little effect any further out from the anomalies).

SUMMARY:

An anomaly with 1000 times the impedance of the surrounding area causes very little change in the current paths. To deflect a large amount of current to the edges of the array, the anomaly would have to be very large and/or very close to an edge of the array. (Even the three-by-three anomaly only produced small divergence in current paths). Also, more current would probably be deflected to

the surface if one end of the current source was connected in close proximity to the anomaly.

4. Model Summary

The results from this circular array model were much better than the results from the square model. The diagonal, upon which the anomaly was situated, could be determined. The amplitude of the impedance measurements may also determine the anomaly's distance from the center of the array. Clearly, more tests would be required. However, changing the location of anomalies on this model was very time-consuming. A faster, more efficient method would be required. The result was the computer model in section C. Further tests were conducted using that model.

Also, currents are deflected by anomalies, but the deflection is small. Deflections are most noticeable when the anomaly is very close to the surface.

C. The Computer Model

1.Purpose

Now that the results were more positive, more experiments needed to be conducted on the circular array. However, the current process was very time-consuming. Soldering and removing resitors took time, as did measuring the impedances for all the diagonals using the multimeter. A quicker method of obtaining measurements was needed. Hence a computer model was developed, which would simulate the circular array model.

At this time, since an anomaly was now detectable, we needed to examine how the impedance method could be used to assess gastric emptying. That was a major concern while designing the remaining experiments. To keep this document straightforward, the analysis is presented in chapter IV.

2. Description of Model

Instead of measuring the impedances directly, the computer solution would determine the equivalent impedance between any two points on the surface, using Kirchoff's voltage laws. A voltage source and the voltage laws were chosen (instead of a current source and Kirchoff's current laws) to cut down on the number of computations. In the square-resistor array, there would be 20 x 20 cells (400 individual loops) along with the loop containing the voltage supply (a total of 401 equations). In contrast, there were

21 x 21 or 441 nodes in the same array, and hence up to 441 different equations using Kirchoff's current laws.

A typical cell had four resistance values. One current, I_1 would be assigned to the cell, and four other currents would surround the cell (I_2 through I_5). Consider the figure below.

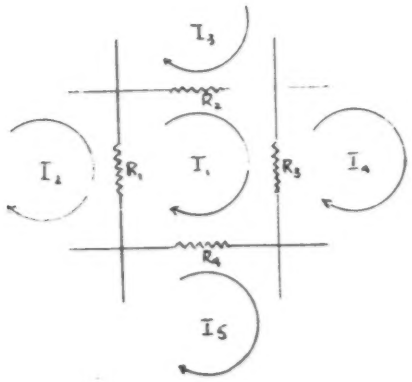

Figure 27: Currents and resistances of a single cell in the square resistor array model

The voltage equation for a cell would take on the form of

$$0 = (R_1 + R_2 + R_3 + R_4)I_1 - R_1I_2 - R_2I_3 - R_3I_4 - R_4I_5$$

Even still, there were too many equations to solve by hand, so a matrix was developed to hold the equations. It took the form of

$$V = \Sigma * I$$

where V was a vector with 401 elements. All of them were zero except for the last one, which would hold whatever value the voltage source would output. (This value is

arbitrary as shown later on.) Z was the impedance matrix (401 by 401 elements), and I was a vector of the same dimensions of V.

$$\begin{bmatrix} 0 \\ 0 \\ \vdots \\ 0 \\ V_s \end{bmatrix} = \begin{bmatrix} & ZZ...Z & \\ & ZZ...Z & \\ & & \\ & & ZZ...Z \\ ZZ & \cdots\cdots\cdots\cdots\cdots & ZZ \end{bmatrix} \begin{bmatrix} I_1 \\ I_2 \\ \vdots \\ I_n \\ I_s \end{bmatrix}$$

The square matrix model was chosen over the circular model due to the Z matrix. It would be too time-consuming to enter all the separate elements individually, even if this is to be done once. A more efficient way to enter the values would be to use the square array and then develop an algorithm for filling in the non-zero elements.

At the same time, a simpler method needed to be developed to enter the resistor values. There were 21 rows of horizontal resistors in the model (or 21 x 20 resistors) plus there were 20 rows of vertical resistors in the model (20 x 21 resistors). The total would be 840 separate resistors. To save time, these could be generated by the program since most of them were 100 ohm resistors in our experiments.

However, what if the model became more complicated? A more accurate representation of the human body would include separate impedances for tissue, bone, air and so on.

Entering all of these resistor values individually would be very time-consuming. A better method involved looking at the array as a set of 400 cells. Then the user would only need to enter one value of resistance for each cell. The program would then take these values and massage them before putting them into their proper location in the Z matrix. By carefully choosing the cells, the number of resistances to be entered could be reduced. To save time further, an initial set of cell resistances was stored in the program. It included very large impedances to represent the air space (the cells located in the corner of the square resistor array since the circular array yielded better results), and 'background' impedances (the 100 ohm resistors in the model). The cell-concept made the program easier to use.

It was intended that some form of graphical interface could be developed as well. A diagram on the terminal would show the model using the initial set of data. Then, the user could enter a value of resistance and simply point to the cells which were to have that resistance. In this manner, the user could quickly and efficiently use the model to represent any configuration desired. However, time did not permit this development and other problems were solved instead.

A major problem was space restriction. A four-hundred-by-four-hundred matrix of reals (integers would not provide the necessary accuracy) would take a lot of memory to store. To solve for this initially, a much simpler model was

developed. It contained thirteen cells instead of 400 and was arranged in the form of a circle (or diamond). Another problem was the time-restriction. A traditional solution to the problem would be to take the inverse of the Z matrix and solve for I.

$$Z^{-1}V = I$$

Then once I was known, the equivalent impedance could be determined by dividing the current in the outer loop by the voltage of the supply. Moreover, at this point, it could be seen that the value of the voltage supply was arbitrary. The current induced by a supply of 6 volts would be twice the current induced by a supply of 3 volts. The equivalent impedance doesn't change. Now to form the inverse of a fourteen-by-fourteen matrix involved some time. (At this point, the focus was still to solve the problem for the simpler model first.) However, to form the inverse of a four-hundred-by-four-hundred matrix would be much more computationally intensive and time-consuming. Different methods were looked at to forming the inverse, but the problem would still be computationally difficult. The problem required more thought.

It was noted that the only current that it was necessary to solve for, was the current in the loop containing the voltage supply. Once that was known, then

the equivalent impedance could be readily determined. What was required was a solution to the specific equation:

$$V_{source} = I_{source} * Z_{eq}$$

Or

$$V_{source} = I_{11}*0 + I_{21}*0 + \ldots + I_{source} * Z_{eq}$$

The latter equation could be obtained if the Z matrix was reduced row by row, using Cramer's rule, until the only non-zero element in the last row of the Z matrix was the one in the last column. Thus a reduction method was coded which would result in a new equivalent Z matrix with only zeroes in the elements left of the main diagonal. (It was not even necessary to perform the reduction on the right half of the matrix, since the only interest was in obtaining the equivalent impedance of the entire matrix.) This formed the basis of the program that was to be developed.

One complication was left to solve before the working solution for the thirteen-cell model was implemented. The problem involved accuracy. The program would at times explode while massaging the values in the Z matrix. Upon closer examination, it was discovered that the computer would sometimes represent zero as a very small number (a limitation that can occur due to roundoff errors and the computer's finite accuracy when storing numbers). This

caused problems since at different times in the solution, a small number would be divided by another small number. Now if the numerator was to be effectively zero, then the result of this division is zero. If the denominator was smaller than the numerator, however, the result could be any value up through infinity. A check was included in the program to solve this problem.

After that was solved, the program worked very well for the thirteen-cell case. A physical thirteen-cell model was constructed and the results compared vary favorably with those calculated by the program. The next step was to apply this method to the much larger twenty-by-twenty model.

This was no longer a microcomputer problem, due to the space limitations described earlier. The program was moved onto the mainframe (HP 9000). Also, the C programming language was used to circumvent matrix problems encountered using Fortran. This entailed learning both the UNIX operating system and the C programming language.

After this was done, the impedances for the four hundred cells were entered and the program run. One major modification was made. The positions of the diagonals were also entered into the program. Now, instead of rerunning the program once for each equivalent impedance, the program would generate equivalent impedances for an entire set of diagonals.

Initially, the program took days to run. Tests had to be carefully designed, since the results would not be back

in minutes. Also, as the Hewlett Packard mainframe was a time-sharing system, the time and computer usage was clearly unacceptable. Moreover, there were times when the system needed to be freed for other users, and at times, the program was halted before completion. Once again, a more efficient algorthm was required.

The matrix is very sparse. Only a small part of it had non-zero elements. Research followed on a variety of sparse matrix techniques. However, none of the situations applied to this matrix. Most of the nonzero elements were situated on the main diagonal. But there were also four other nonzero diagonals. As well, since the last row of the matrix defined the voltage loop for the electrodes, it was difficult to predict which columns in this row would be nonzero in advance.

Research into sparse matrices did not yield a workable solution; a manual approach was again attempted. From this approach came the modifications to the algorithms. First, to save computations, elements were checked for a zero result. If zero would be the result (which could be determined without actually doing the enitre calculation), then the calculation was not performed and zero stored as the element. This resulted in faster processing times but the solution still took time.

Instead of checking for a zero result, another approach was implemented. To reduce checking time, all the individual elements which could possibly be changed by the

massaging process was identified. Then calculations were only performed for these individual elements.

During these improvements, a careful eye was kept to make sure none of these changes would invalidate the final result. The objective was to cut down on unnecessary calculations, but only at the expense of speed, not at the expense of accuracy.

It was primarily these improvements which yielded the final product: a computer solution which now solved the problem in a matter of minutes instead of days. With this accomplished, it was now possible to run tests with any configuration desired.

These tests showed it was possible to determine the times at which the stomach reached maximum and minimum volumes through the use of surface measurements.

3. Experiments

A primary concern was to ensure that the computed impedances matched the measured values from the analog model. This was actually performed in a number of experiments, but for brevity, only experiment 4 is detailed.

At this point, greater emphasis was placed on assessing gastric emptying. Chapter IV contains a detailed description of this analysis. Experiments 5 and 6 are based on the probe-location method, while experiments 7 and 8 are based on the changing-volume method.

In experiment 5, the resistance of the anomaly was reduced. It was now only five times the value of the surrounding media. The aim was to determine if these smaller anomalies could still be detected and located.

Experiment 6 looked at how accurately the position of a single-cell anomaly could be determined. This is a follow-up on an earlier experiment which suggested that the anomaly's distance from the center of the array may be determined by the amplitude of the impedances measured.

In experiment 7, the anomaly is enlarged to a block of five cells in width and length (to represent the stomach). Stomach contraction is then modelled by successively removing a column of resistors. The goal was to determine whether the change in volume is detectable, and whether the direction of contraction can be determined.

Experiment 8 models the stomach in a more circular fashion. The anomaly takes on four sizes. The objective is to determine what changes in impedance result from this expansion/contraction.

Experiment 4: COMPUTED IMPEDANCES VS MEASURED IMPEDANCES

OBJECT:

The object is to verify that the computed values are similar to the ones measured on the circular resistor board model. Actually, this was done on a continuous basis during the computer program design. When the values for the no-anomaly situation agreed, the computer model was modified to simulate the same situations as in experiment 2.

APPARATUS:

Computer Model

Anomaly resistors = 1 M ohms

Normal resistors = 100 ohms

Probes are on the surface

PROCEDURE:

Computer simulation was run using the situations described in experiment 2. Namely, the no-anomaly case, and the three single-anomaly cases (row 10 col 10, row 5 col 17, and row 12 col 19).

RESULTS:

The computed figures were tabulated in the first half of table 2. These were then subtracted from their corresponding values from experiment 2, to arrive at the differences in figures displayed in the second half of table 2. The largest difference between computed and measured

values is just under five ohms. Possible sources of errors include the use of 1 M ohm in the computer versus the use of open-circuit resistance in the circular board model. However, since the possible error in resistor value is also approximately 5 ohms, this difference is minor.

SUMMARY:

The results obtained using the computer model are very accurate (in that they match the values obtained using the physical analog model).

Diagonal	None	R10C10	R5C17	R12C19
1	306.21	335.33	307.54	307.70
2	263.05	291.91	264.44	264.44
3	247.96	276.46	249.47	249.26
4	241.47	269.58	243.16	242.68
5	239.56	730.08	241.54	240.72
6	241.47	684.51	243.87	242.60
7	247.96	283.53	250.94	249.09
8	263.05	298.83	266.76	264.19
9	306.21	342.13	310.65	307.38
10	225.31	261.37	230.54	226.50
11	256.42	292.63	264.22	257.68
12	307.57	343.83	317.85	308.88
13	234.61	270.95	247.85	235.98
14	296.70	333.07	317.62	298.18
15	232.66	269.07	265.95	234.25
16	303.78	340.17	345.18	305.54
17	250.78	287.15	1181.91	252.70
18	216.05	252.36	1106.42	218.37
19	293.17	329.36	1171.68	295.95
20	245.68	281.77	255.85	248.98
21	218.49	254.35	224.60	223.05
22	301.11	336.79	306.17	307.08
23	259.66	295.17	263.78	267.28
24	247.07	734.06	250.29	258.59
25	243.88	650.34	246.45	263.88
26	247.07	275.15	249.19	1278.03
27	259.66	288.09	261.50	1291.02
28	301.11	329.80	302.80	337.72
29	218.49	247.45	220.04	244.88
30	245.68	275.16	247.07	258.33
31	293.17	322.98	294.48	302.05
32	216.05	246.22	217.29	222.06
33	250.78	281.48	251.97	255.03
34	303.78	334.79	304.96	307.36
35	232.66	263.99	233.82	235.63
36	296.70	328.37	297.86	299.28
37	234.61	266.63	235.77	236.82
38	307.57	339.87	308.75	309.58
39	256.42	289.03	257.63	258.25
40	225.31	258.42	226.58	226.89

Diagonal	None	R10C10	R5C17	R12C19
1	1.28	-1.37	1.34	-4.31
2	-3.76	-3.67	-2.14	3.13
3	-2.20	-1.72	0.00	-1.50
4	4.33	4.66	-2.52	0.77
5	3.81	-1.57	1.81	1.25
6	-0.66	-1.47	-2.78	-3.95
7	2.40	2.61	3.51	1.79
8	0.47	-2.22	-1.10	-0.20
9	-1.60	0.48	3.37	-4.23
10	4.99	-0.79	-4.65	-4.98
11	-0.67	-4.08	-2.69	-4.51
12	3.26	-4.99	-1.79	3.50
13	-0.46	0.74	3.20	-0.59
14	-2.98	-3.19	3.73	3.23
15	-2.51	4.10	3.25	2.32
16	0.57	-4.67	-3.23	-3.72
17	-3.97	-2.56	4.54	-3.94
18	-4.72	-4.32	2.87	-2.57
19	-3.98	-4.92	-2.33	0.95
20	-2.85	-1.73	-1.54	3.36
21	2.81	0.47	3.56	-2.24
22	-2.55	-4.62	-0.79	2.41
23	-3.89	-1.95	-1.71	0.38
24	-3.43	3.29	-3.53	-4.88
25	2.79	0.73	-3.76	-0.94
26	0.96	0.11	1.93	-4.75
27	2.91	2.96	1.11	4.31
28	3.12	-0.84	0.25	1.49
29	-1.18	-0.47	-4.72	1.39
30	4.85	-1.95	-0.08	-0.20
31	-2.59	-0.16	-2.80	-4.52
32	3.55	3.32	2.28	-3.68
33	-4.50	-2.05	-3.09	-2.57
34	1.64	0.77	-1.44	0.99
35	-1.70	-1.84	-0.32	0.13
36	-0.89	1.29	-4.91	1.73
37	1.08	-3.77	-2.18	-4.47
38	-0.78	2.54	-3.34	-0.75
39	3.86	-3.74	0.55	2.28
40	-2.69	-4.01	-2.00	2.53

Table 2: a) the computed values of impedances (in ohms) and b) the differences in impedance between computed and measured values (in ohms)

Experiment 5: IMPEDANCE USING SMALLER ANOMALY

OBJECT:

The anomaly can be detected (from a previous experiment) when the anomaly has high impedance, but is the anomaly detectable when it has a much lower impedance? The impedance of the stomach, bone, and other tissue in the body does not differ by a factor of 10^4. Are these at least detectable, using the computer model? How much do they influence the results?

APPARATUS:

Computer Model

Anomaly resistors = 500 ohms

Normal resistors = 100 ohms

Probes are on the surface

PROCEDURE:

An anomaly of 500 ohms is placed at certain columns along row ten in the array. Specifically, columns 10, 15, 17 and 19. The surface impedances of these cases were then calculated.

RESULTS:

The results are graphed in figure 28. There is very little difference in measured impedances for each situation. The largest difference (between the case when the anomaly is farthest from the edge and the case when the anomaly is

closest to the edge) is a little over ten ohms, and only in one diagonal.

SUMMARY:

Anomalies with five times the impedance of the surrounding media are largely undetectable. The largest difference between an anomaly virtually at the surface and an anomaly at the center is approximately ten ohms along one diagonal. Size of the anomaly may change this conclusion. Once again, clear imaging is at best, a remote possibility.

The advantage is that the results are largely uninfluenced by such small differences. (From previous experiments, differences reached the level of 1 k ohm, while here the differences are around one to two ohms on the average.) Consider for example, an x-ray image which included tissue as well as bone in the diagram. The shape of one would effectively obscure the details of the other, and the x-rays would not be able to yield a picture of bone which is surrounded by tissue. Similarly, if a high-impedance probe was attached to the stomach lining, it would be desirable if the surface impedances were not affected by the amount of tissue in the plane as well as the location of the probe.

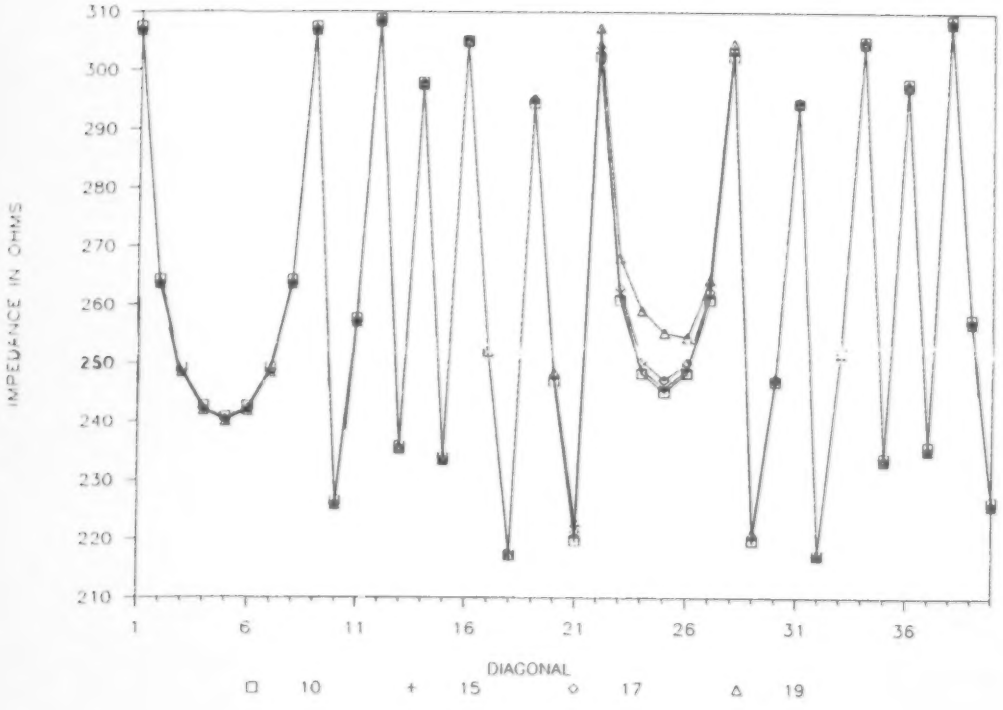

Figure 28: Diagonal impedances of the circular resistor array model when the single anomaly has five times the resistance of the other cells

Experiment 6: IMPEDANCES AS SINGLE-CELL ANOMALY IS MOVED

OBJECT:

Earlier on, it was shown that the angle of an anomaly could be detected. At the time, it was suggested that the radial distance may also be determined through the amplitude of the impedance differences. The object of this experiment was to see if the above is true and if so, how accurately could this radial distance be determined.

APPARATUS:

Computer Model

Anomaly resistors = 1 M ohms

Normal resistors = 100 ohms

Probes are on the surface

PROCEDURE:

The single-cell anomaly was positioned in row 10 and varied from columns 10 through 20. The impedances were then calculated by computer and tabulated.

RESULTS:

Figure 29 shows the results. The measured impedances vary primarily in two ways: first in the main diagonal on which the anomaly is situated (as expected from previous experiments) and in the diagonals largely perpendicular to the main diagonal.

In the latter case, the jumps only occur in diagonals one to six and in the situations when the anomaly is located in columns ten to fifteen. The impedance changes are significant; between 0.7 and 1 k ohm. It is hypothesized that these spikes are the result of the 'flat' edge on the top of the circle model. By the time the anomaly reaches column 16, the effect of the flat edge is lessened. On a human body, the flat edges would be replaced by a smooth curve with no sharp corners. The model may have to be modified to compensate for this effect.

Along the main diagonal, the impedance spike ranges from 0.7 to 1.3 k ohms. The impedance differences for each case are not uniform. In fact, they almost seem like quantum leaps with a difference of approximately 0.1 k ohms between different levels. Six different 'layers' can be identified as follows:

layer 1 : anomaly is in columns 10 through 12

layer 2 : anomaly is in columns 13 and 14

layer 3 : anomaly is in columns 15 and 16

layer 4 : anomaly is in columns 17 and 18

layer 5 : anomaly is in column 19

layer 6 : anomaly is in column 20

Figure 30 contains a graphical representation of the different layers. The layers become thinner as the anomaly approaches the edge. This is expected, since an anomaly close to the edge is much easier to detect than one closer to the center of the array.

SUMMARY:

The radial distance of the anomaly can be approximated to one of six layers, using the surface impedance of the diagonal which contains the anomaly.

It is suspected that the shape of the model may also result in impedance spikes in the diagonals perpendicular to the main diagonal. Flat edges and sharp corners may affect the results. As the array uses more and more cells, this effect will probably be reduced. Some changes may be necessary in the model to test for this. It is not known at present whether these changes may also make the aforementioned layers less discrete.

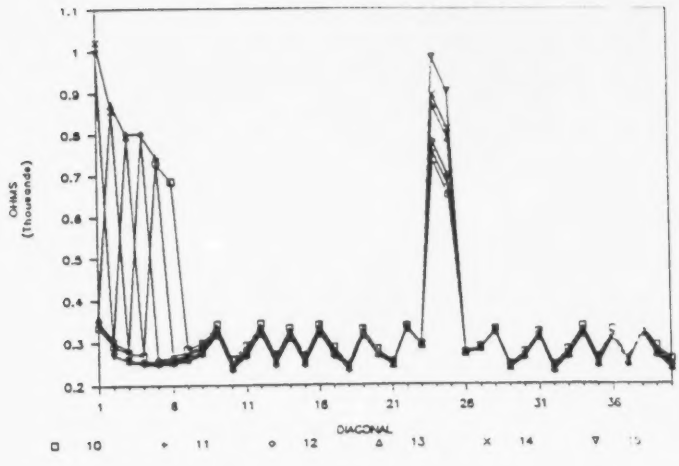

a)

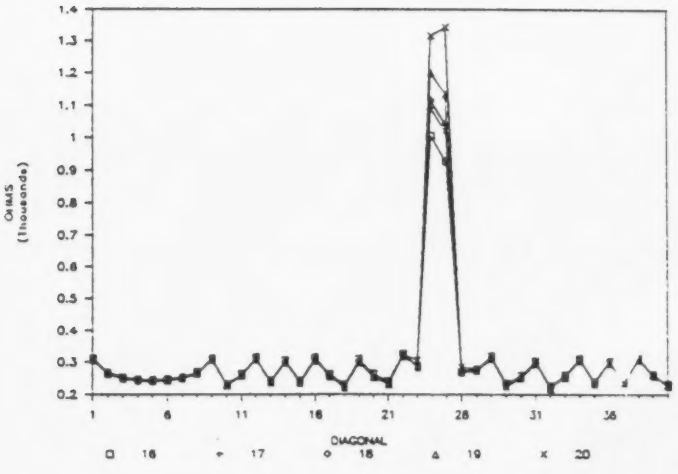

b)

Figure 29: the impedances calculated as the single-cell anomaly is moved a) from column 10 to column 15, and b) from column 16 to column 20

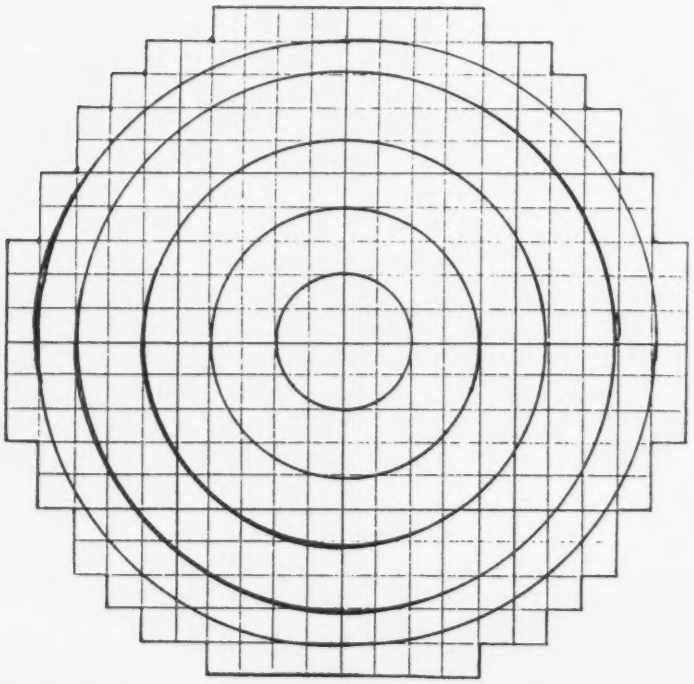

Figure 30: the six layers in the model. An anomaly passing between layers causes an increase in impedance of approximately 0.1 k ohms.

Experiment 7: IMPEDANCES AS COLUMNS ARE REMOVED

OBJECT:

A different approach was taken at this point. Instead of tracking a single-cell anomaly, it was desired to note the effects of a larger anomaly. Specifically, if a larger anomaly were to change size, would its contraction and direction be detectable?

This would be the situation if instead of using a probe, the patient were to ingest a solution or substance of high impedance. Depending on the time intervals, different volumes would be contained in the stomach.

Also, if an anomaly were to change sizes largely in one direction, could this direction be determined from surface measurements?

APPARATUS:

Computer Model

Anomaly resistors = 1 M ohms

Normal resistors = 100 ohms

Probes are on the surface

PROCEDURE:

A five-by-five block was placed within an otherwise uniform array of resistors. The resistances within the block were 1 M each while the resistances outside the block were 100 ohms each. Impedances across diagonals were

calculated. The block was situated between columns 10 to 14 inclusive and rows 10 to 14 inclusive.

Single columns were then removed from the block anomaly and replaced with resistances of 100 ohms each. In the first case, column 10 was removed and the block occupied columns 11 to 14 (between rows 10 to 14). Impedances across the diagonals were then taken again.

Next, column 11 was replaced, so that the block was now situated between columns 12 to 14 and measurements taken again. This process was repeated until only column 14 remained. Impedances were recorded for this last case as well.

RESULTS:

In every situation, the maximum impedance across a given diagonal coincided with the five-by-five block. As the size of the block decreased, so did the measured impedance.

The diagonals with the largest impedance differences between maximum and minimum block sizes were at right angles to the direction of expansion. Large differences were noted in diagonals four to six (vertical alignment and passing through the block) while smaller differences were noted in diagonals 24 to 26 (horizontal alignment while still passing through the block).

SUMMARY:

A change in block size is detectable at the surface. Furthermore, this change is noticeable in any diagonal, since all diagonals show a difference in measured impedance between each of the five sizes. The difference may be small; an expansion by one column may produce only a difference of less than two ohms in a surface diagonal.

The direction of expansion/contraction may be determined by noting the diagonal which shows the largest change in impedance. However, unlike the situation of a moving single-cell anomaly, the contraction is along an axis which is perpendicular to this diagonal. This axis coincides with the diagonal showing the minimum change in impedance.

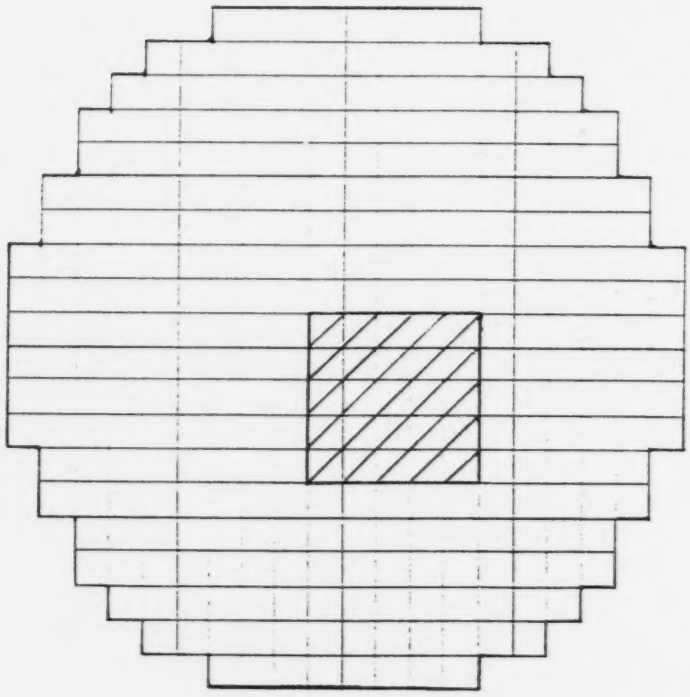

Figure 31: location of the single multiple-celled anomaly

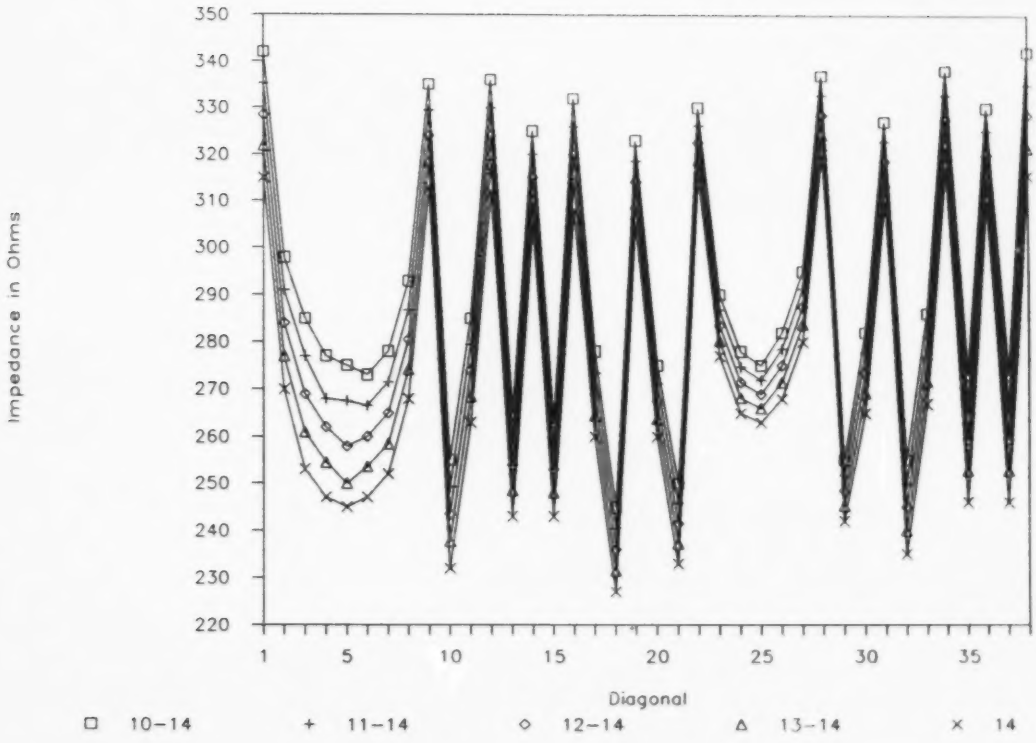

Figure 32: computed impedances as the anomaly contracts one column at a time

Experiment 8: IMPEDANCES AS ANOMALY CHANGES SIZE

OBJECT:

The previous experiment used a square block. Since the stomach is more rounded, this experiment uses a more round anomaly.

The object of this experiment is to note specifically the amount of change in impedance measured when the anomaly changes sizes from a diameter of zero to a diameter of five cells (5/20 th the diameter of the 'abdomen' array).

APPARATUS: Computer Model
Anomaly resistors = 1 M ohm
Normal resistors = 100 ohms
Probes are one-deep

PROCEDURE:

The anomaly is centered at row 13 column 14 (see diagram), to simulate an off-centered stomach. The anomaly takes on four sizes with diameters of zero cells, one cell, three cells, and five cells.

The resistances of the anomaly is purposefully set at a much larger value than the other resistances; therefore the differences in impedances measured represent the maximum value that can be expected.

RESULTS:

The accompanying graph shows the impedances as predicted by the computer model and the differences between successive sizes. Also, in this experiment, the angle of the diagonal (rather than the number) is used as a horizontal axis on the graph. The purpose of this is to better approximate a continuous case, rather than the discrete one in the model.

There are three key observations. First, the difference per change in volume is much smaller than the single-cell situation. Whereas the latter resulted in differences in the hundreds of ohms, the changes here are in units of ohms and tens of ohms. These small figures emphasize the need to use accurate instruments and the need for careful measurement to reduce errors due to leads, contact impedance and stray capacitances.

Secondly, the impedance at any single set of probes increases with each increase in size of the anomaly. This implies that any probe set can be used to detect the maximum and minimum sizes of the stomach.

Thirdly, the differences between successive states become more pronounced as the edges of the anomaly approach the edge of the array. This could also be caused by the larger change in volumes as the anomaly expands (say from a diameter of three cells to one of five cells).

SUMMARY:

As the anomaly changes sizes from a minimum of zero to a maximum of thirteen cells, the changes in impedances expected are quite small. This necessitates careful attention to errors and accurate impedance meters. Any set of probes may be used to determine maximum and minimum sizes since an increase in volume corresponds with an increase in impedance measured in all cases. Finally, a larger change in impedance is measured at the probes when the size of the anomaly is larger (and thus closer to the edge of the array).

Since the ratio of resistances between anomaly and surrounding matter is higher in the computer model than the ratio expected in humans, the results represent the maximum differences that can be measured on a true abdomen.

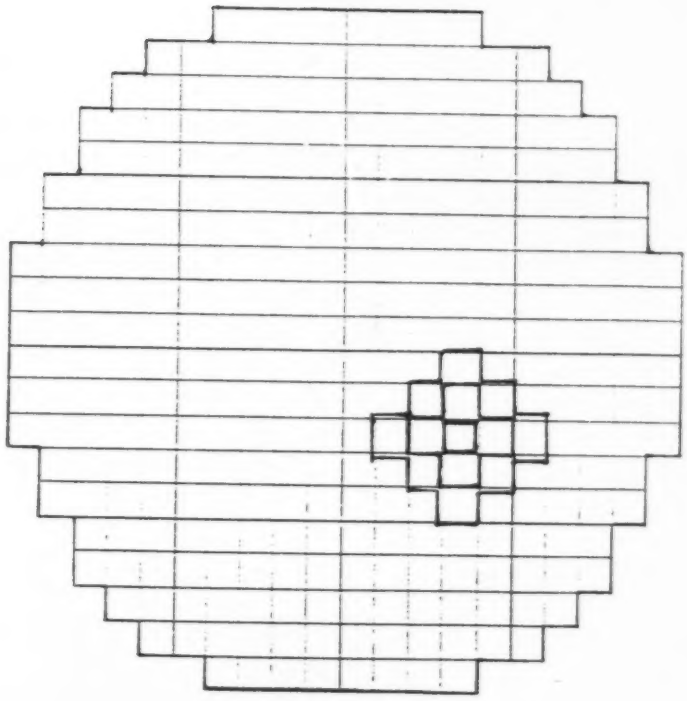

Figure 33: the three different sizes in the anomaly

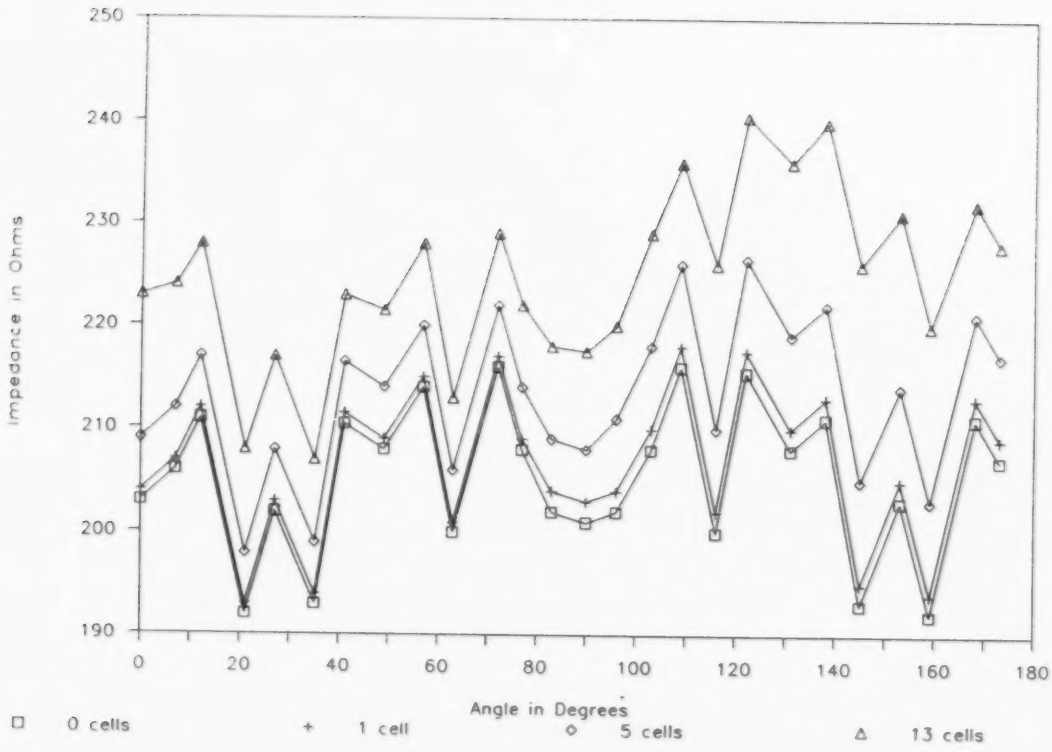

Figure 34: computed impedances as the anomaly's radius changes

4. Summary of Model

The computer model retained the advantages of the previous analog models. In addition, the model could be easily changed to represent any configuration of impedances. The model was also very time-efficient; taking only minutes to calculate the impedances for any set of diagonals.

Once the model was developed, a number of experiments on gastric emptying were performed. In the probe-location method, a single-cell anomaly of high impedance could be located in one of six different levels.

Using the changing-volume method, the volumes of high-impedance fluid decreases as the stomach empties. The volume changes are detectable using surface readings. In addition, if the contraction is largely along one axis, then this direction can be determined as well.

D. The Electrolytic Model

1. Purpose

As some of the previous experiments showed, the flat edges and sharp corners of the circular model may affect results. In general, how do the results from the discrete model compare to the continuous situation found in the human body?

The electrolytic model was designed in response. The focus was on the shape of the graph that would result, more than the actual values of the impedances measured.

2. Description of Model

The electrolytic model consisted of a round plastic container. It was filled with an aqueous solution of water and salt (to represent the surrounding media of previous models). Finally, a cylindrical piece of plastic was placed in the solution to represent the anomaly.

Probes were then placed into the solution at diametrically opposite points, and as close as possible to the edge without touching the edge. There was no desire to have the impedance of the plastic container affect the measurements.

3. Experiments

Only one experiment was carried out with this model. The results from this confirmed what was already suspected. Changes would be required in the resistor board model.

Experiment 9: SURFACE IMPEDANCE FROM AN ELECTROLYTIC MODEL

OBJECT:

The object is to compare the results of the computer discrete model to the results of a more continuous model.

APPARATUS:

Electrolytic Model

Hewlett Packard 3490A Multimeter

PROCEDURE:

The electrolytic model was constructed and the impedances between diametrically opposite points were measured. Each set of measurements were separated by an angle of six degrees with zero degrees being due North and advancing counterclockwise. The direction for zero was arbitrarily chosen, with the intent of establishing a common reference point.

RESULTS:

The results are graphed in figure 35. Except for minor differences of 0.5 ohms (possibly due to experimental error), the graph is a smooth curve, as expected. When compared to the equivalent thirteen-cell situation in experiment eight, the major difference is the lack of impedance spikes in this graph.

SUMMARY:

Clearly, some modifications would be necessary to the discrete model to reflect these differences.

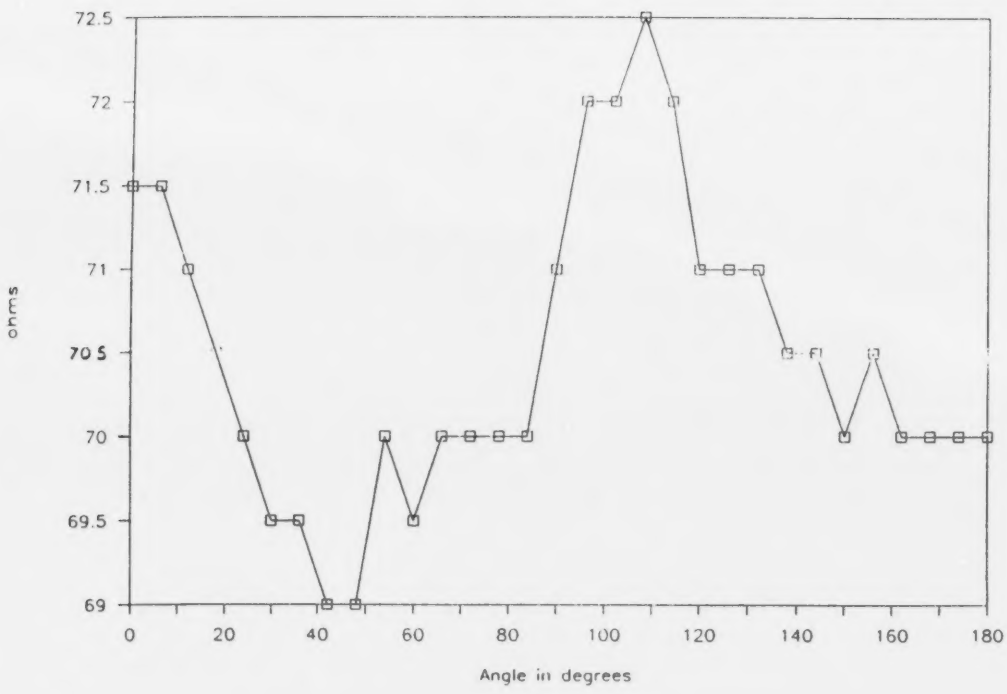

Figure 35: measured impedances for the electrolyte (continuous) model containing a circular, continuous anomaly with a diameter of one-quarter the diameter of the model

4. Summary of Model

The graph resulting from this model lacked the impedance spikes of the graph from the computer model. The computer model would need to be changed.

E. Modifications to the Resistor Board Model

1. Purpose

The results of the electrolytic model did not agree with the results of the resistor model. This necessitated some modifications.

2. Description of Modifications

The first modification that came to mind would be to increase the number of cells in the model. As the cells got smaller, it would be reasonable to expect that the measured results would more accurately reflect the results of the continuous model. The number of computations would increase but not become more difficult. However, before such a solution was to be implemented, a careful re-examination of the model may suggest better modifications. If the modifications could be easily implemented without a high increase in the number of computations, then clearly this would be a better solution.

The second modification had already been implemented. Rather than graph using diagonal number, angle was chosen for the horizontal axis. This was necessary as the angle between different diagonals in the model was not uniform in all cases.

Also, to better simulate a circle, the impedances were normalized by length. In the electrolytic model, the container was a circle, and the distance between the two

probes was always the same. In the discrete model, this was not the case. The length between the probes was calculated in units of cells (the length of the hypotenuse of a right triangle whose height and base represented the number of cell rows and columns between the two probe points).

These two helped quite a bit, but the single largest problem still remained: the impedance spikes in the discrete model were not present in the continuous model. This problem required quite some thought.

The first clue came with the identification that the spikes occurred always at the same diagonals. That was coupled with the previous observations concerning the 'flat edges' and 'sharp corners' of the array. The flat edges produced the smooth curve found in all graphs. The 'outside' corners produced the maximums and the 'inside' corners produced the minimums. Since outside and inside corners alternated fairly frequently spikes occurred in the waveforms.

But while outside and inside corners were different visually, what specifically was different about them? Why did one create a maximum and the other a minimum? The answer was in the number of resistors connected to the corner. Outside corners are at the junction of two resistors, whereas inside corners are at the junction of four. Flat edges were at the junctions of either two or three resistors. As the number of branches in a parallel

circuit greatly affects the equivalent impedance, this answer seeemed to make sense.

But if this is the problem, then how does one circumvent it? The only way was to ensure that all the junctions had an equal number of resistors connected to it. In the electrolytic model, the probes could be placed close to the edge of the solution, but could not be placed exactly on the edge. Precise placement was clearly impossible. This led to the idea that impedances needed to be measured close to the edge but not quite on the edge. In effect, probes would be placed 'one-deep' (one layer deep into the array). These new points were always at the junction of four resistors.

3. Experiments

With these modifications, the final set of experiments were performed on the computer model. The resulting waveforms were much better approximations to the electrolytic model.

Experiment 10 uses the computer model to solve for the impedances when the probes are placed one layer deep. In addition, the impedances have been normalized by the diagonal length.

The final experiment considers a stomach filled with a high-impedance solution. As the stomach contracts, some of the solution enters into the duodenum. It is important to determine the times when the stomach reaches maximum or

minimum volume (irrespective of the duodenum). This last experiment examines whether the expanding duodenum affects the measurements from the stomach.

Experiment 10: THE EFFECT OF NORMALIZATION AND THE USE OF ONE-DEEP PROBES

OBJECT:

The goal of this experiment was to determine whether the application of two correction factors to the resistive model might yield results which were more compatible with the results from the electrolytic model.

Probes were positioned one layer deep within the array, thereby always resting on the junction of four resistors while still being close to the edge of the array (to simulate surface measurements).

Secondly, the impedances were normalized using the probe-to-probe distance (diagonal). Since the array is made up of discrete elements (instead of continuous) joined together in rectangular fashion, the diagonal length varies. The impedance measured across a longer diagonal will be higher than the impedance across a shorter diagonal. To correct for this, impedances were normalized with respect to diagonal length.

APPARATUS:

Computer Model

Anomaly resistors = 1 M ohm

Normal resistors = 100 ohms

Probes are one-deep

PROCEDURE:

The angle assigned to zero degrees is changed here to better reflect geometry standards (zero degrees being due east).

The diagonals are outlined in figure 36. The computer data was modified so that the new endpoints of the diagonals reflected the "one-deep" levels. Two situations from experiment 8 were considered. The first situation considered the thirteen-cell anomaly while the second situation dealt with the one-cell anomaly.

RESULTS:

The results are graphed in figures 37 and 38. Impedances from the one-deep case have fewer spikes than the corresponding impedances using the computer model alone. The spikes are even less noticeable (and hence more similar to the electrolytic model's) when the impedances are normalized using the diagonal length.

In addition, the impedances were plotted separately onto figure 39. As noted before, the impedance of the thirteen-cell anomaly is higher than the impedance of the one-cell anomaly for all diagonals. The maximum and minimum volumes of the stomach can be ascertained at any diagonal. Some diagonals yield better results (higher differences) though.

SUMMARY:

The modifications yield a waveform which better approximates the one in the electrolytic model. Also the basic conclusions from previous resistor board experiments are still valid. The times at which the anomaly reaches maximum and minimum volumes can be determined through surface impedance measurements.

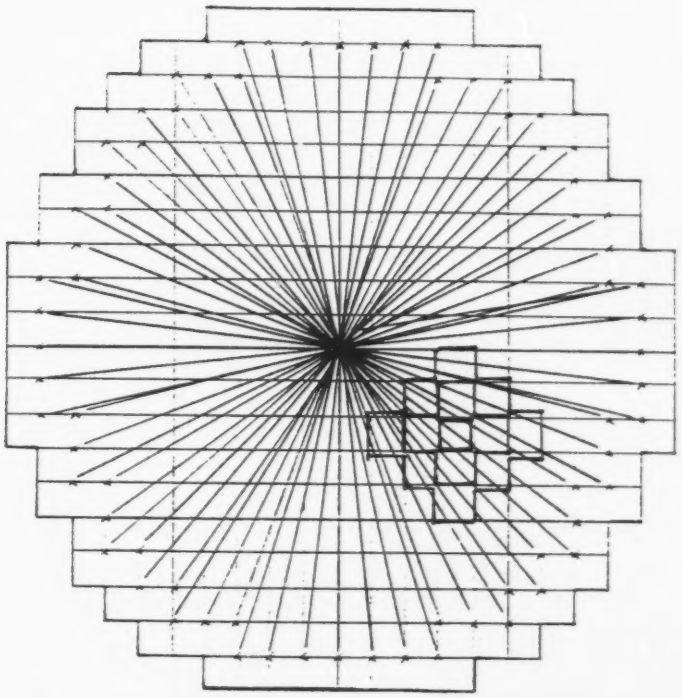

Figure 36: one-deep probe locations in the circular model

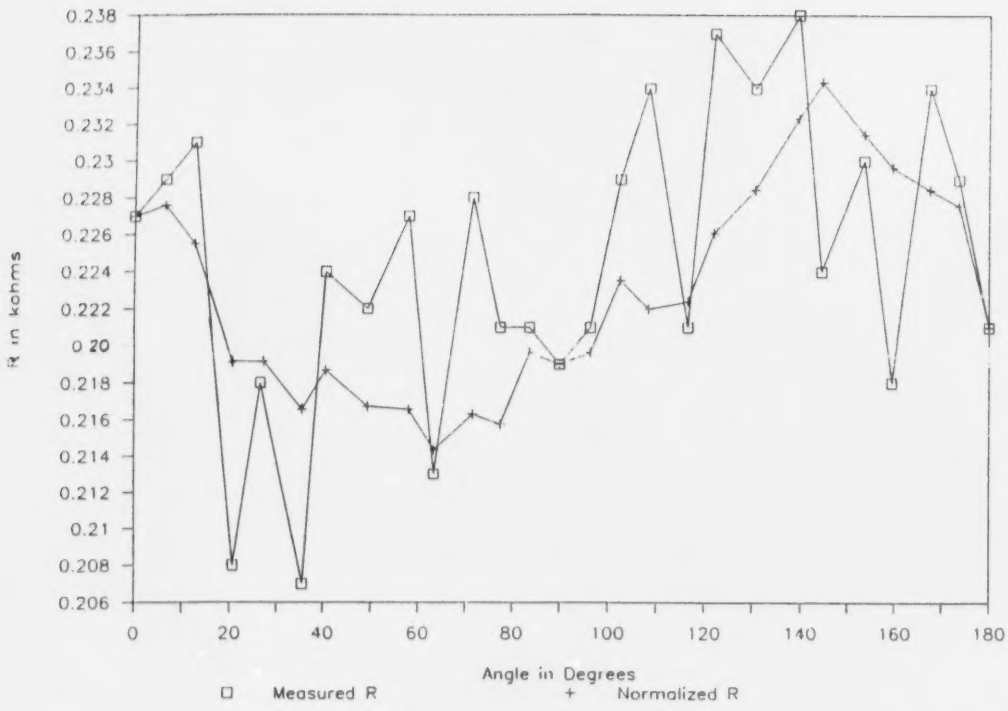

Figure 37: computed impedances for the 13-cell anomaly when probes are located one layer from the edge of the array, both before and after normalization

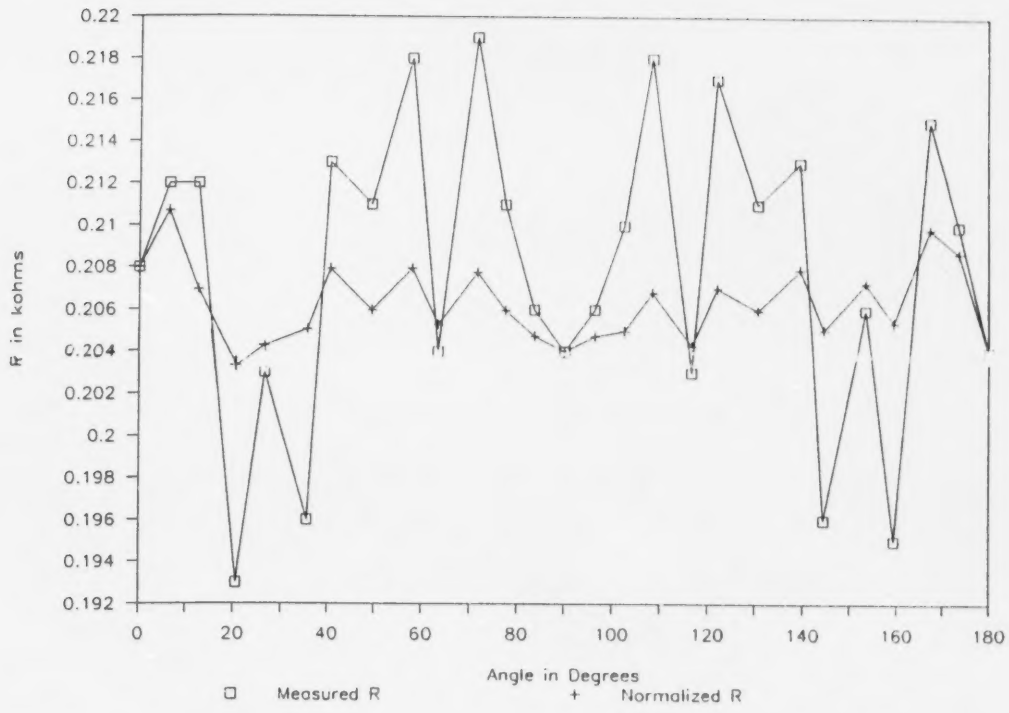

Figure 38: computed impedances for the one-cell anomaly when probes are located one layer from the edge of the array, both before and after normalization

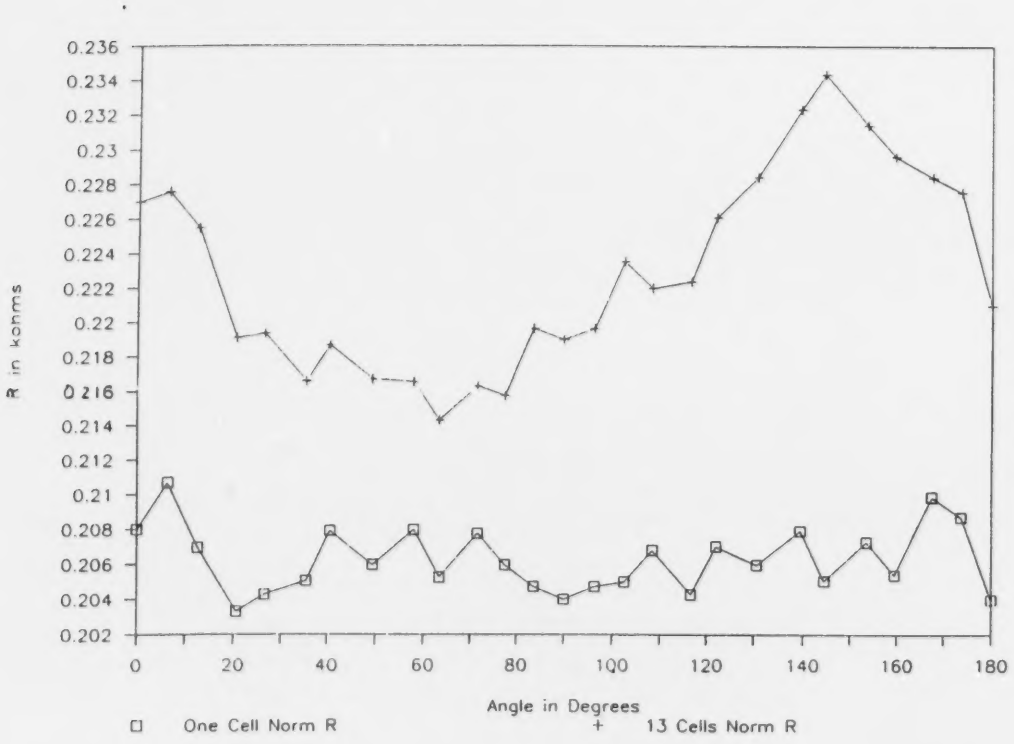

Figure 39: normalized impedances for the 13-cell and one-cell anomalies

Experiment 11: IMPEDANCES AS STOMACH CHANGES SIZE

OBJECT:

In a previous experiment, the changes in impedances were noted as the anomaly expanded in a circular fashion from a diameter of one to five cells. In this experiment, the anomaly sizes are chosen to more accurately display the change in the stomach size during digestion. In essence, as if the patient has digested food with a high resistivity. Since the food may also show up on the duodenum (which may also lie in the plane of interest), the model also takes into account the effect of food in the duodenum on the measurements.

APPARATUS:

Computer Model

Anomaly resistors = 1 M ohm

Normal resistors = 100 ohms

Probes are one-deep

PROCEDURE:

The model centers the stomach at a radius of roughly one-third the radius of the abdominal cavity. The model then assumes three different states, each characterizing a different stage in the digestive cycle of the stomach.

When the food first enters the stomach, the stomach enlarges to maximum size (in our model, the diameter reaches

9/20 th of the abdominal diameter). None of the food reaches the duodenum yet since the food is undigested.

As food is digested, the stomach reaches the average state (stomach diameter is 7/20 th of the abdominal diameter in this model). Some of the food goes into the duodenum (approximated in the model as 1/20 th the abdomen's diameter).

The stomach then contracts to a minimum size as the food passes out of it. At this point, the amount of food in the duodenum reaches a maximum. In the model, the stomach and duodenum diameters are 5/20 th and 2/20 th the diameter of the abdomen. The three different states are diagrammed in figure 40. Impedance probes were then placed one layer deep in the computerized array and the impedances were calculated.

RESULTS:

Figure 41 contains the resulting measurements. 'Min', 'Avg' and 'Max' refer to the three different sizes of the stomach.

The impedances were normalized over the length of each diagonal. The average for each set of measurements was graphed versus the angle of the diagonal.

The first thing to note is that the impedance of the maximum state is always greater than that of the average state. In turn, the latter is always greater than the impedance of the minimum state for any set of probes. This

implies that the expansion of the duodenum does not significantly alter the effects caused by the contraction of the stomach.

Secondly, the greatest amount of difference between impedance measurements is observed at an angle of zero and 173 degrees. In the model, these diagonals approximately bisect both the stomach and duodenum as well as detail the direction of expansion in the stomach. Thus, in practical cases, it is expected that the angle along which the stomach expands can be determined. This conclusion may require modification if the actual stomach does not expand in circular fashion (as in the model).

In the simulation, the difference in impedances between the max and min states never goes below fourteen percent (of the min value). At times, the max value will be more than twice as large as the min value. Thus, even after allowing for small errors in the actual case, the change in impedance is easily measurable.

Finally, the length of the diagonal is significant. The graph lines are smoother once the measurements are normalized by length.

SUMMARY:

An expanding duodenum does not offset the effects of a contracting stomach. The impedance of a smaller stomach (with larger duodenum) is never greater than the impedance of a larger stomach with a smaller duodenum.

The direction of stomach expansion coincides with the angle bisecting stomach and duodenum.

Finally, the impedance changes are easily measureable, with smaller changes in impedances between successive angles when the results are normalized with respect to probe-to-probe distance (length of diagonal).

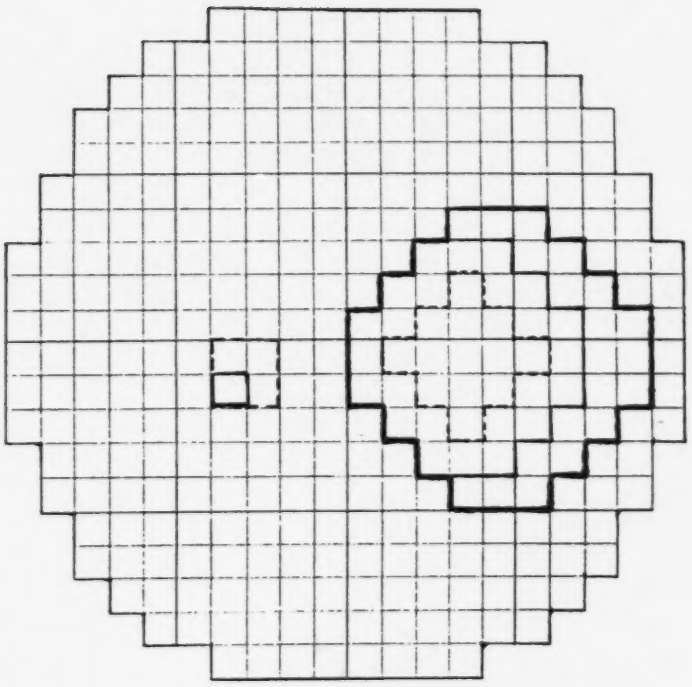

Figure 40: the three different sizes for the stomach and duodenum

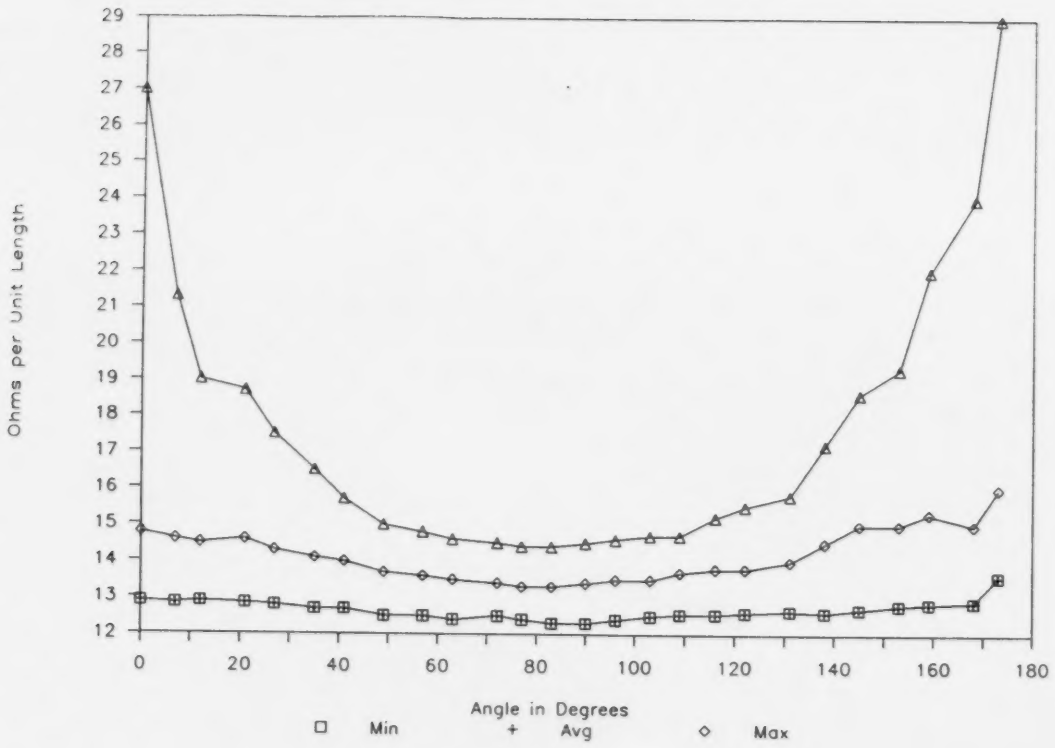

Figure 41: the normalized impedances for the different stomach and duodenum sizes

4. Summary of Modifications

The experiments in this section had better results than the ones in previous sections. Specifically, the impedance electrodes are connected at points which are one layer away from the edge of the array and the impedance values are normalized using the diagonal length. The result is a smoother waveform (less impedance spikes) which better approximates the results from the electrolytic model.

The last experiment also shows that an expanding duodenum does not offset the effects of a contracting stomach.

IV. ASSESSMENT OF GASTRIC EMPTYING

This chapter details how surface impedance measurements can be used to assess gastric emptying. Though this was actually developed during the course of this study, including this in chapter III seemed confusing.

Two methods, in particular, were developed. In gastric emptying, it is important to have some way of measuring the volume of the stomach's contents. The stomach can be thought of as a container of changing shape. The volume can be measured in a number of ways.

An indirect method would estimate the volume by recording the dimensions of the container. For instance, if the stomach were cylindrical, its volume could be determined given its height and the radius of its circular base. A more direct method woul measure the volume of the actual contents.

Both methods can be used to assess gastric emptying. This discussion uses area instead of volume, since the experiments are in two dimensions. It is a simple matter to extrapolate into three dimensions, by substituting volume calculations for the area calculations.

LOCATION OF SINGLE-CELL ANOMALY

The first method assesses volume indirectly. The area (that the stomach covers in the plane of interest) can be calculated if the radius of the circular stomach is known.

Consider the situation when a small object of high impedance is attached to the stomach wall. This can be accomplished noninvasively by inserting a tube down through the patient's throat into the stomach. The end of the tube which connects to the stomach wall, can have a small object of high impedance attached to it. If the impedance of this object is much higher than the impedance of the surrounding tissue and stomach contents, then we have the situation of a "single-cell" anomaly placed within the torso.

Experiments in this study have shown that the location of this anomaly can be determined using surface impedance methods. We can easily determine when the stomach reaches maximum and minimum volumes by noting when the anomaly comes closest to and moves farthest from the surface of the torso.

To assess in-between volumes (as the stomach expands or contracts), the surface impedance measurements can be compared against the values obtained using the computer model. If the values are different, then the computer configuration can be changed and new impedance values calculated again. This successive approximation method may yield not only an accurate value for stomach area, but also a good estimate of the stomach shape as well.

Another modification which would help to define the shape of the stomach, would be to use more than one anomaly.

Mapping each anomaly's location may result in a more accurate picture of the stomach's shape and size.

VOLUME OF A HIGH-IMPEDANCE FLUID

The difficulty of the previous method lies in the high amount of computing that is required. Also, since the stomach contains air as well, stomach size may not be a direct measure of actual stomach volume.

This second method assesses volume more directly, and without the need for computation.

First a known volume (say 100 mL) is ingested by the patient. Then the impedances are measured immediately. Then, the patient ingests an additional volume of the fluid (say 100 mL more). Then the impedances can be measured again. In this manner, a graph of volume vs average impedance can be drawn. It is important that the time period between successive additions is very short, so as not to give the stomach time to start emptying the fluid.

After the patient has ingested the entire amount, the impedance probes are left on and monitored at different times. These measurements result in an impedance vs time graph.

Then, by matching the impedances between the filling and emptying cycle, a third graph of volume vs time can be extrapolated. This last graph would effectively show the emptying cycle.

This method has several advantages over the location method. First, no computed results are necessary. Secondly, this method involves volumes (in three dimensions) rather than areas, in two dimensions.

V. Conclusion

Originally, impedance computed tomography was examined as a noninvasive method for obtaining a cross-sectonal image of the human torso. The images produced, however, had very low resolution, and hence the method was not used to assess different volumes. However, the method still yielded useful information, and the impedance method was used to assess gastric emptying.

During the course of the study, a number of different models were designed and constructed. The computerized model was very adaptable, supporting any number of test configurations. It also proved very efficient; the program rapidly calculated the impedances between a set of point-pairs. These points could be located anywhere on the array, and any two points could be selected as a pair. This was achieved only after developing an efficient computer algorithm which could efficiently solve the very large impedance matrix, while still maintaining the solution's validity by accurately handling very small matrix values. The computerized model also simulated better the results obtained from a more continuous situation (as found in the actual human body), by selecting the points to be one-layer deep from the edge of the model (as opposed to on the surface of the model), and by normalizing the impedances measured by the distance between the two points.

The experiments yielded two significant results. First, impedance methods determine very accurately the times when the stomach has reached maximum and minimum volumes. Even an opposing action in the duodenum does not change this result. Secondly, the impedance probes should be placed along the axis of expansion for best results. In the case of the stomach, this direction of expansion is largely known.

With these results, two different methods were developed to assess gastric emptying. The first method detected a small anomaly's position within the abdominal cavity. A probe could be inserted containing the anomaly. This anomaly would then be attached to the stomach wall. Then, using impedance methods, the location of the anomaly (and hence the location of the stomach wall) is determined. Using a number of measurements, a number of different volumes (as the stomach empties) can be determined, and gastric emptying can be assessed.

The second method involves measuring the volume of a high-impedance food ingested by the patient (as opposed to measuring the location of the stomach wall). A series of impedance measurements can be recorded for different volumes in the patient. Then, as the food leaves the stomach, the resulting impedances can be correlated with the earlier measurements to yield a gastric-emptying curve.

FOOTNOTES

[1] D. C. Barber and B. H. Brown, "Applied Potential Tomography," 1984 p. 723.

[2] Ibid., p. 723.

[3] A. D. Seagar et al., "Theoretical limits to sensitivity and resolution in impedance imaging," Clinical Physiology and Physiological Measurements," 1987, Vol. 8, suppl. A, p. 13.

[4] Y. Kim and H. Woo, "A prototype system and reconstruction algorithms for electrical impedance technique in medical body imaging," Clinical Physiology and Physiological Measurements," 1987, Vol. 8, suppl. A, p. 66.

[5] D. G. Gisser et al., "Current toics in impedance imaging," Clinical Physiology and Physiological Measurements," 1987, Vol. 8, suppl. A, p. 39.

[6] Barber and Brown, "Applied Potential Tomography," p. 724.

[7] Ibid., p. 725.

[8] Ibid., p. 729.

[9] Ibid., p. 725.

[10] Ibid., p. 725.

[11] Ibid., p. 726.

[12] Y. Kim and H. Woo, p. 66.

[13] H. M. Powell et al., "Impedance imaging using linear electrode arrays," Clinical Physiology and Physiological Measurements," 1987, Vol. 8, suppl. A, p. 110.

[14] W. R. Breckon and M. K. Pidcock, "Mathematical aspects of impedance imaging," Clinical Physiology and Physiological Measurements," 1987, Vol. 8, suppl. A, p. 77.

[15] T. J. Yorkey and J. G. Webster, "A comparison of impedance tomographic reconstruction algorithms," Clinical Physiology and Physiological Measurements," 1987, Vol. 8, suppl. A, p. 55.

[16] Y. Kim and H. Woo, p. 68.

[17] Barber and Brown, "Applied Potential Tomography," p. 729.

[18] Ibid., p. 728.

[19] Ibid., p. 728.

[20] Ibid., p. 728.

[21] D. N. Smith, "Determination of impedances usng numerous simultaneous currents (DINSC) - system design and practial applications," University of Edinburgh and Lothian Health Board, UK p. 69.

[22] H. M. Powell et al., "Impedance imaging using a linear electrode array," University of Sheffield, p.90.

[23] Barber and Brown, "Applied Potential Tomography," p. 729.

[24] Ibid., p. 723.

[25] H. Griffiths and A. Ahmed, "A dual-frequency applied potential tomographic technique: computer simulations," Clinical Physiology and Physiological Measurements," 1987, Vol. 8, suppl. A, p. 103.

[26] D. G. Gisser et al., p. 41.

[27] Y. Kim and H. Woo, p. 64.

[28] B. H. Brown et al, "Applied Potential tomography: possible clinical applications," Clinical Physiology and Physiological Measurements," 1987, Vol. 8, suppl. A, p. 110.

[29] Ibid., p.113.

BIBLIOGRAPHY

Barber, D. C. and A. D. Seagar "Fast reconstruction of resistance images" Clinical Physics and Physiological Measurements, 1987, Vol. 8, Suppl. A, 47-54

Barber, D. C. and B. H. Brown "Applied potential tomography", 723-733

Barber, D. C. and B. H. Brown "Recent Developments in Applied Potential Tomography - APT" Proceedings of the 9th Conference in Information Processing in Medical Imaging, June 1985, Vol. 10, No. 14,

Bates, R. H. T. "Full-wave computed tomography Pt. 1: Fundamental theory" IEE Proceedings, Vol. 131, Pt. A, No. 8, Nov. 1984, 610-615

Breckon, W. R. and M. K. Pidcock "Mathematical aspects of impedance imaging" Clinical Physics and Physiological Measurements, 1987, Vol. 8, Suppl. A, 77-84

Brown, B. H. and A. D. Seagar "Applied Potential Tomography - Data Collection Problems" IEE International Conference on Electric and Magnetic Fields in Medicine and Biology, Publication 257, December 4-5, 1985, 79-82

Brown, B. H. and A. D. Seagar "The Sheffield data collection system" Clinical Physics and Physiological Measurements, 1987, Vol. 8, Suppl. A, 91-97

Brown, B. H., D. C. Barber and A. D. Seagar "Applied potential tomography: possible clinical applications" Clinical Physics and Physiological Measurements, 1985, Vol. 6, No. 2, 109-121

Conway, J. "Electrical impedance tomography for thermal monitoring of hyperthermia treatment: an assessment using in vitro and in vivo measurements" Clinical Physics and Physiological Measurements, 1987, Vol. 8, Suppl. A, 141-146

Dawids, S. G. "Evaluation of applied potential tomography: a clinician's view" Clinical Physics and Physiological Measurements, 1987, Vol. 8, Suppl. A, 175-180

Ettinger, K. V. and A. C. MacKay "The Principle of Electric Field Tomography and its Application to Selective Read-out of Information from Peripheral Nerves", University of Aberdeen, UK, 64-68

Eyuboglu, B. M., B. H. Brown et al. "Localisation of cardiac related impedance changes in the thorax"

Clinical Physics and Physiological Measurements, 1987, Vol. 8, Suppl. A, 167-173

Gisser, D. G., D Isaacson and J. C. Newell "Current topics in impedance imaging" Clinical Physics and Physiological Measurements, 1987, Vol. 8, Suppl. A, 39-46

Griffiths, H. and A. Ahmed "A dual-frequency applied potential tomography technique: computer simulation" Clinical Physics and Physiological Measurements, 1987, Vol. 8, Suppl. A, 103-107

Griffiths, H. and A. Ahmed "Applied potential tomography for non-invasive temperature mapping in hyperthermia" Clinical Physics and Physiological Measurements, 1987, Vol. 8, Suppl. A, 147-153

Kim, Y. and H. W. Woo "A prototype system and reconstruction algorithms for electrical impedance technique in medical body imaging" Clinical Physics and Physiological Measurements, 1987, Vol. 8, Suppl. A, 63-70

Mangnall, Y. F., A. J. Baxter et al. "Applied potential tomography: a new non-invasive technique for assessing gastric function" Clinical Physics and Physiological Measurements, 1987, Vol. 8, Suppl. A, 119-129

Minard, R. A., B. S. Robinson and R. H. T. Bates "Full-wave computed tomography Part 3: Coherent shift-and-add imaging" IEE Proceedings, Vol. 132, Pt. A, No. 1, Jan. 1985, 50-57

Murphy, D., P. Burton et al. "Impedance imaging in the newborn" Clinical Physics and Physiological Measurements, 1987, Vol. 8, Suppl. A, 131-140

Parker, Dennis L. and Paul D. Clayton "Computed Tomography: The Revolution in Computer Based Medical Imaging" M.D. Computing, 1984, Vol. 1, No. 1, 36-46

Powell, H. M., D. C. Barber and I. L. Freeston "Impedance imaging using linear electrode arrays", Clinical Physics and Physiological Measurements, 1987, Vol. 8, Suppl. A, 109-118

Powell, H. M., D. C. Barber and I. L. Freeston "Impedance Imaging using a Linear Electrode Array", University of Sheffield, 88-92

Sakamoto, K., T. J. Yorkey and J. G. Webster "Some physical results from an impedance camera" Clinical Physiology

and Physiological Measurements, 1987, Vol. 8, Suppl. A, 71-76

Seagar, A. D., T. S. Yeo and R. H. T. Bates "Full-wave computed tomography Part 2: Resolution limits" IEE Proceedings, Vol. 131, Pt. A, No. 8, November 1984, 616-622

Seagar, A. D. and R. H. T. Bates "Full-wave computed tomography Part 4: Low-frequency electric current CT" IEE Proceedings, Vol. 132, Pt. A, No. 7, November 1985, 455-459

Seagar, A. D., D C Barber an B H Brown "Theoretical limits to sensitivity and resolution in impedance imaging" Clinical Physiology and Physiological Measurements, 1987, Vol. 8, Suppl. A, 13-31

Smith, D. N. "Determination of Impedances using Numerous Simultaneous Currents (DINSC) - System Design and Practical Applications" University of Edinburgh and Lothian Health Board, UK, 69-73

Tarassenko, L., M. K. Pidcock et al. "The Development of Impedance Imaging Techniques for Use in the Newborn at Risk of Intra-Ventricular Haemorrhage" IEE International Conference on Electric and Magnetic Fields in Medicine and Biology, Pub. 257, 1985, Dec. 4-5, 83-87

Vresilovic, E. J., S. R. Pollack and C. T. Brighton "Theoretical Determination of Electric Fields and Current Densities in Long Bone Fractures during 60 kHz Electrical Stimulation with Skin Electrodes" IEE International Conference on Electric and Magnetic Fields in Medicine and Biology, Pub. 257, 1985, Dec. 4-5, 44-47

Yorkey, T. J. and J. G. Webster "A comparison of impedance tomographic reconstruction algorithms" Clinical Physics and Physiological Measurements, 1987, Vol. 8, Suppl. A, 55-62

Yorkey, T. J., J. G. Webster and W. J. Tompkins "An optimal impedance tomographic reconstruction algorithm" IEEE/Eighth Annual Conference of the Engineering in Medicine and Biology Society, 1986, 339-342